



The origin of Mn and Y annuli in garnet and the thermal dependence of P in garnet and Y in apatite in calc-pelite and pelite, Gagnon terrane, western Labrador

Panseok Yang and Toby Rivers

Department of Earth Sciences, Memorial University of Newfoundland
St. John's, NF, Canada A1B 3X5 <pyang@mun.ca, trivers@sparky2.esd.mun.ca>

Abstract

X-ray compositional maps and zoning profiles for major and trace elements have been measured in garnet, apatite and epidote-group minerals from calc-pelitic and pelitic schists from western Labrador, by electron microprobe and by laser ablation ICP-MS. High Y abundance in apatite adjacent to resorbed garnet and a decreasing modal abundance of apatite with garnet growth indicate that apatite participates in major rock-forming mineral reactions. Phosphorus concentration in garnet porphyroblasts coexisting with apatite decreases smoothly from core to rim and depends moderately on metamorphic grade. Apatite coexisting with xenotime shows high-Y cores and the concentration of Y in apatite increases with metamorphic grade.

Many of the analyzed garnet porphyroblasts exhibit Y annuli which provide information about different physicochemical processes operating during garnet growth. We describe criteria to fingerprint three of these processes in the analyzed garnets. (i) Yttrium annuli produced by *garnet resorption and regrowth* are characterized by an asymmetric shape with a steeper slope on the inner side of the annulus and by a decoupled variation between garnet-compatible and garnet-incompatible elements at the resorption margin. (ii) Y annuli produced by *breakdown of Y- and REE-rich trace phases* such as xenotime, monazite, apatite and epidote-group minerals are indicated by REE peaks in LREE (monazite, allanite), MREE (epidote), or HREE (xenotime, zircon). (iii) Y annuli associated with *diffusion-controlled growth* occur in garnet with oscillatory textural zoning defined by alternating inclusion-rich and inclusion-poor zones, with increases in concentrations of garnet-compatible elements such as Y and HREE correlating with inclusion-free zones. Mn annuli in some garnets were produced by sporadic local breakdown of Mn-rich epidote and in several cases indicate that thin-section scale equilibrium during annulus formation was not achieved, raising questions concerning the use of Mn concentration as a time marker in garnet growth modeling.

Keywords: garnet, apatite, Y and Mn annuli, phosphorus zoning, REE peaks.

Introduction

Major and trace mineral reaction histories of samples from metamorphic terranes are key to deciphering P - T paths of metamorphism, understanding the composition of metamorphic fluids, and interpreting the ages of metamorphism. Reaction histories have been traditionally interpreted by examination of major element zoning in metamorphic minerals and the study of inclusion suites in porphyroblasts. However, major element zoning commonly does not yield unique results in terms of metamorphic processes and also does not provide information on the involvement of trace minerals. This is especially important with respect to trace minerals that are used for age dating because potentially they may provide an opportunity to date reaction processes. Recently, trace element zoning in garnet has been shown to be a potentially useful monitor of metamorphic processes (Hickmott et al., 1987; Hickmott and Shimizu, 1989; Hickmott and Spear, 1992; Lanzirotti, 1995; Schwandt et al., 1996; Spear and Kohn, 1996; Bea et al., 1997; Chernoff and Carlson, 1999; Pyle and Spear, 1999; Pyle and Spear, 2000), and this subject is explored further in this paper.

Several trace element zoning studies of garnet porphyroblasts have reported individual or multiple Y annuli of variable shape and width in pelitic garnets from greenschist to granulite facies (e.g. Lanzirotti, 1995; Schwandt et al., 1996; Chernoff and Carlson, 1999; Pyle and Spear, 1999). Understanding the origin of these features is important because they may reflect a wide range of metamorphic processes such as resorption of garnet, breakdown of Y-enriched trace minerals, kinetic effects such as changes in growth rate, and/or metasomatic infiltration of Y-enriched metamorphic fluids. Phosphorus and Y are major elements in the minerals apatite ($\text{Ca}_5\text{PO}_4\text{F}$) and xenotime (YPO_4). If the chemical potentials of P- and Y-components in garnet and apatite are buffered by phase relations with these minerals and other silicates in a rock, P and Y zoning in garnet may reveal changes in pressure, temperature, and phase relations of P- and Y-rich minerals during garnet growth.

In this study, the zoning patterns and trace element contents of garnet, apatite and epidote-group minerals are used to investigate the dependence of trace element substitution on metamorphic grade, to decipher various metamorphic processes during growth of the minerals and to identify the former presence of trace minerals that are no longer present in the stable mineral assemblage.

Geological setting and sample description

The seven samples investigated are calc-pelites and pelites from the Paleoproterozoic Knob Lake Group, in

the Gagnon terrane of the Grenville Province of western Labrador, Canada (Fig. 1). Metamorphic grade in this part of Gagnon terrane increases from chlorite-zone in the northwest near the Grenville Front, through the biotite-, garnet-, staurolite- and kyanite-zones, to migmatite-zone (incipient partial melting) in the structurally highest part of the terrane over a distance of about 30 km (Rivers, 1983a). However, the migmatite-zone samples investigated in this study do not show any textural evidence for partial melting because they are pelites and the first vapor-saturated melting reactions take place in semi-pelitic compositions (Rivers, 1983a). In pelitic rocks, the upper limit of the metamorphic field gradient occurs below the vapor-absent muscovite-melting reaction, since the assemblage muscovite-plagioclase-quartz is still stable and the assemblage kyanite-potassic feldspar (\pm secondary muscovite) has not been observed (Rivers, 1983a).

Metamorphism and deformation in the Gagnon terrane are inferred to be a result of northwest-directed understacking of the Gagnon terrane beneath the Molson Lake terrane (Brown et al., 1992; van Gool, 1992; Rivers et al., 1993). This part of the Gagnon terrane underwent two episodes of penetrative deformation during the understacking event (Rivers, 1983b; van Gool, 1992), with S_1 being recorded in the analyzed samples as an internal foliation (S_i) within garnet porphyroblasts and S_2 being the external matrix foliation. The peak of regional metamorphism coincided with the second phase of deformation. Estimates of the peak temperature and pressure conditions during metamorphism were determined with garnet-rim and matrix-mineral compositions (van Gool, 1992). Temperature variation across the metamorphic gradient, calculated using the Ferry and Spear (1978) geothermometer equation, ranges from 450 to 750°C, and associated pressures determined using the garnet + plagioclase + kyanite + quartz and garnet + plagioclase + biotite + muscovite geobarometers of Newton and Haselton (1981) and Hodges and Spear (1982), range from 6 to 11 kbar. van Gool (1992) and Indares (1995) inferred that the rocks followed "hair-pin" shaped P - T paths with an average slope of 1 kbar/50°C for both prograde and retrograde paths, implying a short period of isobaric heating and decompression after attainment of peak pressure conditions. Additional details concerning the geologic setting, phase relations, petrography, and P - T conditions can be found elsewhere (Rivers, 1983a; Rivers, 1983b; van Gool, 1992; Rivers et al., 1993; van Gool and Cawood, 1994; Indares, 1995; Yang and Rivers, 2001).

The mineral assemblages of the seven analyzed samples are given in Table 1. All seven samples contain garnet, biotite, plagioclase, and quartz with or without primary muscovite in the matrix. Garnet nucleated be-

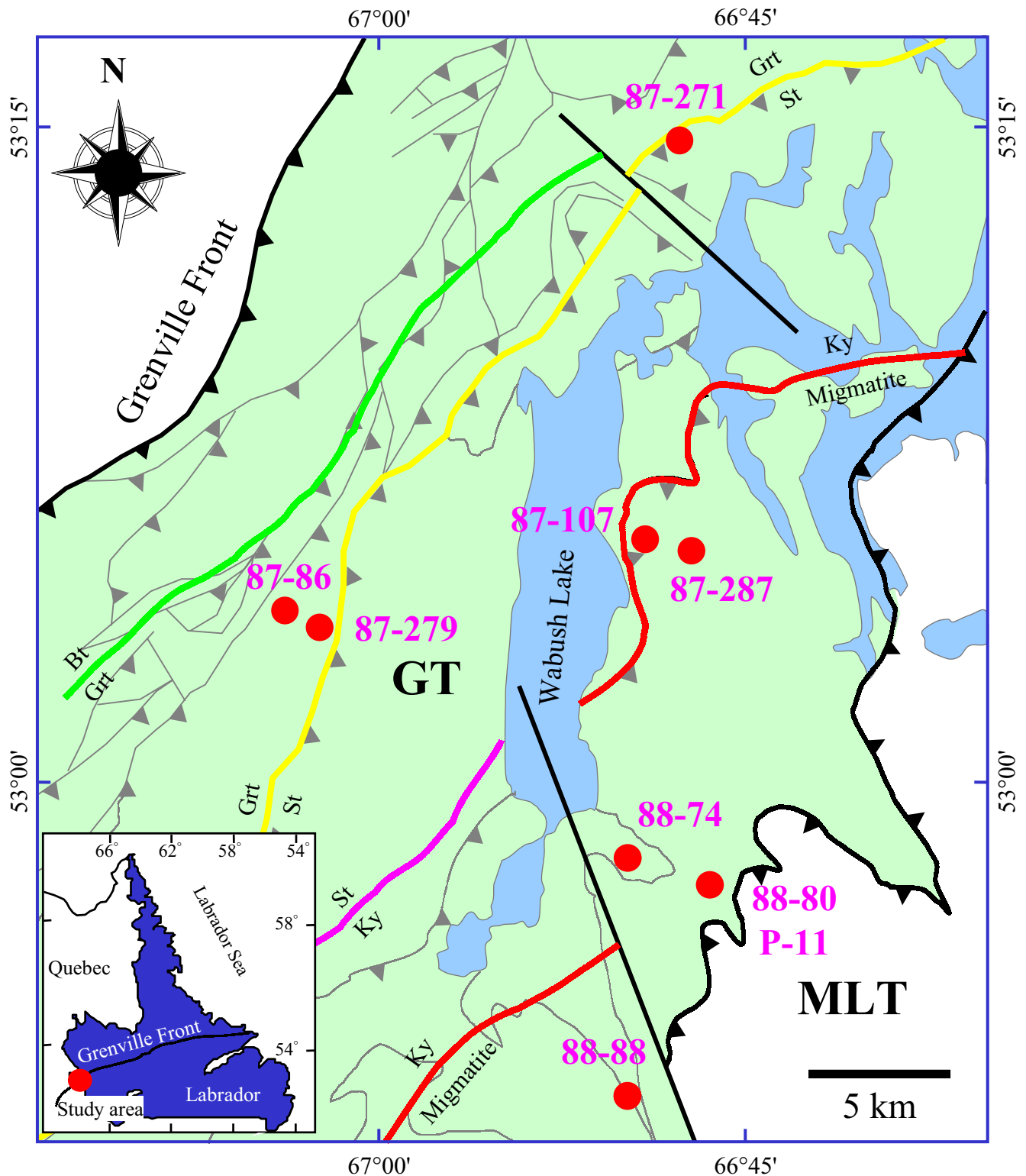


Figure 1. Simplified map of Gagnon terrane, Grenville Province, western Labrador, showing locations of samples used in this study. Metamorphic isograds are from Rivers (1983a) and van Gool (1992). Inset shows the location of the study area with respect to Grenville Front in Labrador. GT: Gagnon terrane; MLT: Molson Lake terrane.

Table 1. Mineral assemblages of the seven samples from western Labrador.

Zones	Samples	Chl	St	Ky	Ep	Ms	Ilm	Rt	Py	Mag	Mnz	Aln	Tur
Garnet	87-86	i			i	×	×						×
Garnet	87-279	i			×	×	×	×	×	×			
Staurolite	87-271	i			i	r	×		×	×			×
Migmatite	87-287				×	×		×	×			×	
Migmatite	88-74			×		×	×	×	×	i	×		×
Migmatite	88-88	i	i	×	i	×	i	×			r	×	×
Migmatite	88-80			×	i	r	i	i	×		×		

Qtz, Bt, Pl, Grt, Zr, Ap, and retrograde Chl are common in all samples. Mineral abbreviations after Kretz (1983).

×-present, blank-absent, i-inclusions in garnet, r-retrograde minerals.

fore the development of the S_2 foliation, and asymmetric pressure shadows around garnet associated with that foliation are common. Garnet porphyroblasts from the garnet- and staurolite-zones are rich in inclusions. Most garnet porphyroblasts from the migmatite-zone are characterized by inclusion-rich cores and inclusion-free rims. Two garnet porphyroblasts (samples 88-74 and 88-88) show an oscillatory textural zoning pattern defined by alternating inclusion-rich and inclusion-free zones. Most garnets investigated in this study are variably resorbed as a result of reaction to form biotite and plagioclase, and show evidence of minor late retrogression to chlorite.

The bulk compositions of all samples except for 88-74 are sufficiently calcic to stabilize epidote-group minerals. Epidote occurs in the matrix as well as in the cores of garnets in sample 87-279 and 87-287, whereas in samples 87-86, 87-271, 88-88, and 88-80 epidote occurs only as inclusions in garnet. Epidote in samples 87-271 and 87-287 is Mn-rich, containing 12 and 7 mol% piemontite respectively. In addition to Mn-rich epidote inclusions, Mn-free epidote with allanite cores occurs both as a matrix mineral and as inclusions in garnet in sample 87-287. Calcite occurs as a minor phase in other samples from the lower grade rocks, but no matrix carbonate or carbonate inclusions in garnet were observed in the samples examined in this study. Apatite, zircon, rutile, and ilmenite commonly occur as minor phases with sparse occurrences of tourmaline, magnetite, allanite, monazite, and pyrite. Ilmenite predominates over rutile in the lower grade samples, with the reverse distribution occurring in the higher-grade rocks, compatible with the inferred P - T path. Magnetite is found in the most Fe-rich samples such as 87-279, 87-271, and 87-287. Graphite occurs only in sample 87-83, and minor chlorite is a retrograde phase in many samples.

Analytical techniques

Major element compositions (Si, Al, Fe, Mg, Mn, Ca) of garnet were determined by energy-dispersive (ED)

X-ray analysis using a LINK ED detector. ED analyses used a cobalt gain calibration and were refined using the LINK ZAF correction program. Analytical conditions included an accelerating potential of 15 kV and a beam current of 20 nA, focused to 1 μm in diameter. Counting times were 60 sec on the samples. The precision of the analyses was generally better than 3% RSD for the major elements.

Apparent concentrations of Ti, P, and Y in garnet and Y in apatite and epidote-group minerals were determined by wavelength-dispersive (WD) X-ray analysis using the Cameca SX-50 electron microprobe at Memorial University of Newfoundland. Operating conditions for garnet analyses included an accelerating potential of 15 kV, a beam current of 300 nA, a beam size 3 μm in diameter, and 60 sec counting times for garnet and epidote-group mineral analyses, whereas for apatite analyses an accelerating potential of 15 kV, a beam current of 20 nA, a beam diameter of 10 μm , and counting times of 120 sec were used. Elemental peaks with no background measurements were standardized using ilmenite (Ti), apatite (P) and xenotime (Y) as standards, resulting in *apparent ppm* which is not ZAF corrected. Although quantitative concentrations of trace elements were not calculated, relative variability of elements across garnet and apatite porphyroblasts provides significant petrologic information. Repeated analyses of an almandine standard revealed that the precision was better than 10% RSD for Ti and 3 % RSD for P and Y. Abnormally high Ti concentrations near Fe-Ti oxides are attributed to fluorescence of Ti X-rays by Fe X-rays (Feenstra and Engi, 1998).

The trace minerals were examined using a SEM in BSE mode. Chemical characterization was aided by qualitative energy dispersive X-ray microanalysis performed with a Link system 860 X-ray microanalyser attached to the SEM. In an attempt to obtain central-section zoning profiles and maps of garnets, the largest garnet in each thin section was analyzed; however, this method does not guarantee a garnet center section. X-ray maps were ob-

tained in WD spectrometry mode, with an accelerating potential of 15 kV and a beam current of 50–100 nA for major elements and 20 kV and 500–700 nA for trace elements using the method described in Yang and Rivers (2001).

Absolute concentrations of P, Sc, Ti, V, Co, Zr, Y, and REE were analyzed in garnet using the LAM-ICP-MS at Memorial University. A complete account of the characteristics and the optimization of this instrument is reported elsewhere (Taylor et al., 1997a; Yang et al., 1999; Yang and Rivers, 2000), and only the key specifications relevant to the present work are given here. The combination of a Q-switched UV laser and optimization of the laser parameters provides a high spatial resolution (10 μm in diameter). However, in order to achieve a balance between spatial resolution and detection limits, the pit size was set at 30–40 μm . Repeated analyses of a glass standard (BCR-2) were used to estimate the precision of the LAM-ICP-MS analyses. This was typically in the range of 6–25 % RSD, depending on the element and its concentration. The LAM-ICP-MS concentration values were calculated using Si concentration obtained by electron microprobe as an internal standard. However, the error bars do not take into account the precision on the electron microprobe determination (estimated at 2% RSD for Si) by error propagation. Analysis spots along each laser traverse were spaced from 30 to ≥ 100 μm apart because of time limitations and the presence of inclusions. Thus, WD profiles give more detailed zoning patterns for Y, Ti, and P. However, LAM-ICP-MS profiles were used when trace element concentrations are below detection limits of WD analysis (~ 100 ppm).

Results

Major and trace element zoning in garnet and reaction histories

Major and trace element zoning patterns in representative garnets from seven samples were examined using

X-ray mapping (Mn, Ca, Y, P), quantitative (Fe, Mg, Mn, Ca) and qualitative (Ti, P, Y) electron microprobe zoning profiles, and laser ICP-MS zoning profiles (Sc, V, Co, Y, Zr, REE). Details of Mn and Cr zoning in garnet from samples 87-86, 87-271, 87-287, 88-74, and 88-88 are discussed in Yang and Rivers (2001). Due to abundant ilmenite and rutile inclusions in most of the examined garnets, interpretation of fine-scale zoning for Ti is difficult. In this study, Sm is considered as a representative for the LREE (Nd, Sm), Gd as a representative for the MREE (Eu, Gd, Tb, Dy), and Yb as a representative for the HREE (Ho, Er, Tm, Yb, Lu). Points labeled A and B in the zoning profiles represent the locations of compositional breaks defined by one or more elements.

Regional metamorphic isograd reactions

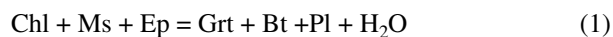
Since detailed discussions of the metamorphic reactions among major phases in metapelitic rocks from the Gagnon terrane have been presented by Rivers (1983a), van Gool (1992) and Yang and Rivers (2001), only metamorphic reactions in calc-pelites are discussed here. For details of staurolite-, kyanite-, and melt-forming reactions, the reader is referred to Rivers (1983a), van Gool (1992), and Yang and Rivers (2001). The changes of mineral compositions and volumes (modes) of minerals in calc-pelites with changing P - T were modeled using the Gibbs method by Menard and Spear (1993). In this study, we use their method to interpret the compositional zoning and the trend of mineral growth and consumption along the P - T path estimated by van Gool (1992). We examine two ways by which the observed zoning could have been achieved, i.e., on the prograde compression-heating path and/or by a combination involving isobaric heating or decompression. The results are summarized in Table 2.

A common mineral assemblage in calc-pelites in the garnet zone in Gagnon terrane is garnet + biotite + plagioclase + quartz + muscovite, with chlorite and epidote occurring as inclusions in garnet. Along the initial compression-heating path, the net reaction is:

Table 2. Predicted changes of compositions of garnet and plagioclase and volumes of garnet from calc-pelite in Gagnon terrane using the Singular model of Menard and Spear (1993) along the P - T path estimated by van Gool (1992).

Reactions	X_{Mg}	X_{Sps}	X_{GrS}	X_{An}	M_{Grt}
1	\uparrow / \uparrow	\downarrow / \downarrow	\downarrow / \downarrow	$\leftrightarrow / \uparrow$	(+) / (+)
2a, b	\uparrow / \uparrow	$\leftrightarrow / \uparrow$	\uparrow / \downarrow	\uparrow / \uparrow	(+) / (-)
3	\uparrow / \uparrow	\downarrow / \downarrow	\downarrow / \downarrow	\downarrow / \downarrow	(+) / (+)
4	\uparrow / \uparrow	\downarrow / \downarrow	\downarrow / \downarrow	\uparrow / \uparrow	(+) / (-)

Symbols on the left and right sides of the forward slash represent directions of compositional changes (X_{Mg} , X_{Sps} , etc.) and change of garnet modal volume (M_{Grt}) along the compression-heating and isobaric heating or decompression paths, respectively.



For this reaction, both the compression-heating and isobaric heating/decompression paths result in the same sense of compositional changes in garnet; i.e., X_{Mg} (Mg/Mg+Fe) increases and X_{Sps} (Mn/Fe+Mg+Mn+Ca) and X_{Grs} (Ca/Fe+Mg+Mn+Ca) decrease with the growth of garnet. X_{An} of plagioclase is nearly constant during the compression-heating path, but increases slightly during isobaric heating or decompression. Reaction (1) would result in the release of Sc, Y, Zr and REE from epidote (Hickmott and Spear, 1992). The exact nature of enrichment of these elements in garnet would depend on the type, abundance and degree of zoning of the epidote-group mineral that was consumed.

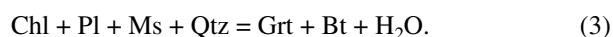
The subsequent evolution depends on whether chlorite or epidote is consumed by reaction first (Menard and Spear, 1993). If chlorite is removed from the assemblage first, the net reaction along the compression-heating path becomes:



Assuming reaction (2a) and a compression-heating path, garnet and plagioclase continue to grow with no variation in X_{Sps} and with increasing X_{Grs} and X_{An} (Table 2). However, along the isobaric heating or decompression paths garnet is consumed in the reaction:



(see Fig. 12d of Menard and Spear, 1993). Thus, evidence of garnet resorption by reaction (2b) indicates a change in the prograde P - T path from compression-heating to isobaric heating. On the other hand, if epidote is consumed first, the assemblage becomes a simple pelite and the net reaction becomes:



The directions of compositional changes in garnet and plagioclase as a result of reaction (3) are independent of the two different P - T paths; in both cases, X_{Mg} of garnet increases and X_{Sps} , X_{Grs} and X_{An} all decrease. The transition from reaction (1) to (3) is characterized by a sharp decrease in Ca in garnet due to the removal of epidote from the assemblage (Menard and Spear, 1993). Garnet growing by reaction (3) is expected to fractionate garnet-compatible elements such as Sc, Y, and HREE originally present in epidote. After both chlorite and epidote are removed, reaction (4) comes into play:



For this reaction, Menard and Spear's model predicts that garnet will be consumed along an isobaric heating path, but will continue to grow along a compression-heating path (reaction goes from right to left), with increasing X_{Mg} and decreasing X_{Sps} and X_{Grs} . Coexisting plagioclase becomes more enriched in the anorthite component if reaction proceeds from right to left.

In this paper, predictions of compositional changes of garnet and plagioclase and associated growth or consumption of garnet are integrated with measured major and trace element zoning patterns and inclusion assemblages to infer the reactions that occurred during the growth of garnet in Gagnon terrane.

Analyzed Samples

87-86 (Garnet-zone). The analyzed garnet from sample 87-86 (0.8 mm in diameter) has an euhedral crystal shape with the left side partly resorbed, as indicated by non-concentric Mn and Y zoning (Figs. 2a, c). X_{Sps} in the garnet decreases monotonically from 0.22 in the core to 0.1 in the rim (Fig. 2e). Both almandine and pyrope components increase continuously toward the rims, and X_{Mg} , although showing a short wavelength periodicity, remains approximately constant (~0.09) from core to rim (Fig. 2e), suggesting only minor change in temperature during growth. Calcium concentration in the garnet shows a step function; X_{Grs} is 0.164 in the core and 0.185 in the rim with a slight discontinuity in the zoning midway between core and rim. The position of the Ca break does not coincide with the point labeled A defined by a marked inflection in Y zoning; on the left side, the Ca break is located just outside the point A, whereas on the right side the break is just inside the point A (Fig. 2f), indicating that the Ca discontinuity is not related to the formation of the Y annulus. Epidote inclusions are absent in the garnet core and the matrix, but occur in the outer part of the garnet where X_{Grs} increases (Fig. 2b).

In contrast to the smooth, nearly monotonic changes in the Mn, Mg, and Fe profiles, Y and Yb (HREE) zoning profiles (Figs. 2f, j) display prominent spikes in concentration between core and rim that correspond to the hexagonal-shaped annuli of high-Y concentration seen in the X-ray map (Fig. 2c). Yttrium concentration in the core of this garnet (1,871 ppm) is the highest among the investigated garnets. In addition to the major peaks, there are a few minor Y-peaks on the profiles that are not apparent on the yttrium X-ray map. Based on the X-ray map and zoning profile, we note that the shapes of the Y annuli are euhedral and symmetrical and infer that they are growth features. Gadolinium (MREE) zoning is decoupled from Y and Yb zoning, and Sm (LREE) increases slightly before decreasing at the rim (Fig. 2j). Ti in this garnet de-

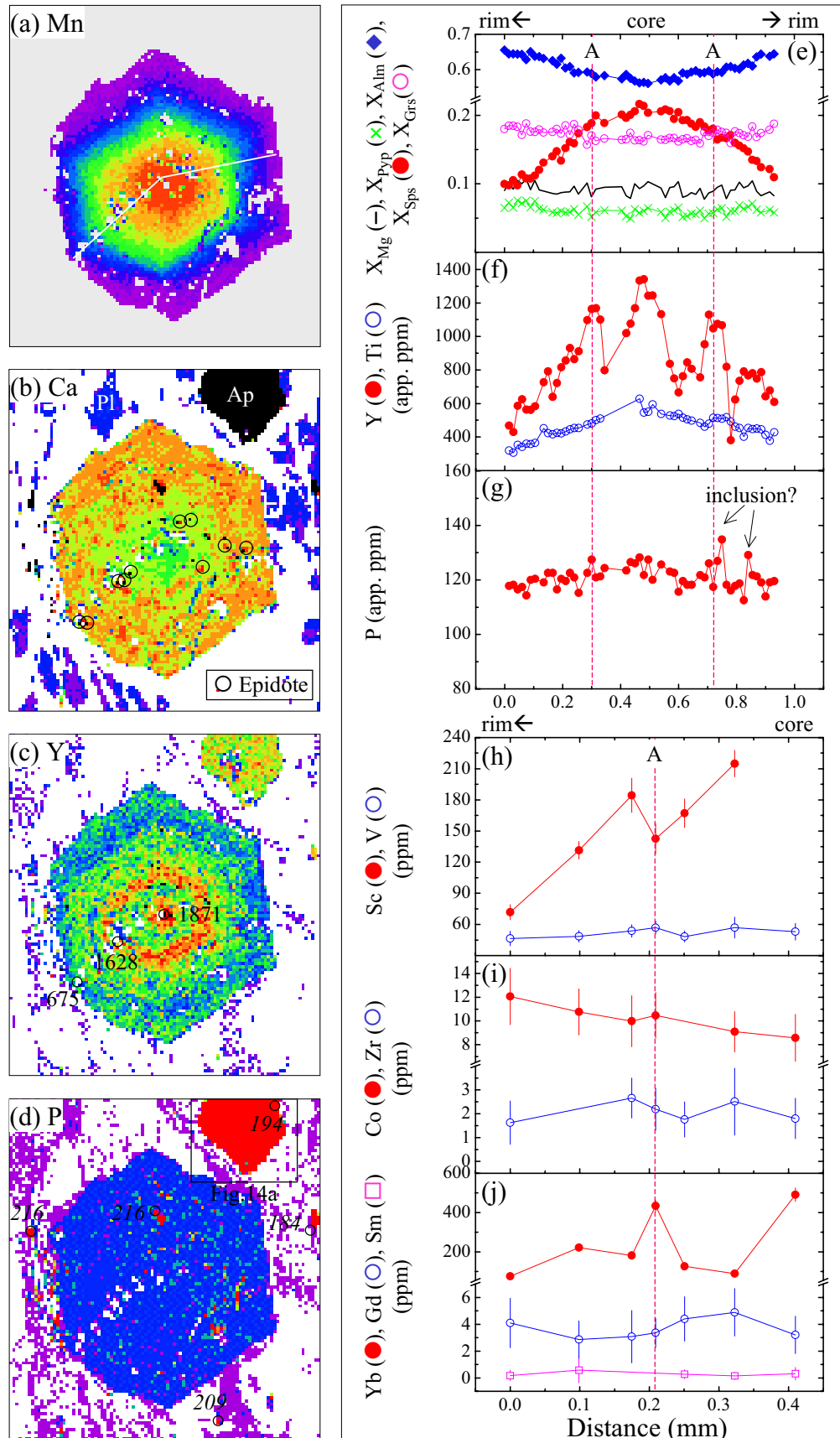


Figure 2. X-ray compositional maps and zoning profiles in garnet from sample 87-86 (garnet zone). (a) Mn map; white lines indicate location of EMP and LAM-ICP-MS profiles. (b) Ca map: circles represent the locations of epidote inclusions in garnet. (c) Y map: representative concentrations of Y determined by LAM-ICP-MS are given in ppm. (d) P map: representative Y analyses of apatite grains determined by electron microprobe are given in app. ppm (italicized numbers). Note that the Y concentrations of apatite grains in the garnet resorption area are higher than those of apatite inclusions in the garnet and matrix apatite. The location of the apatite crystal imaged in Fig. 14a is indicated by the box. In the X-ray maps, warm colors indicate higher concentrations with black for the highest and white for the lowest concentration. (e-g) Rim-core-rim compositional profiles of X_{Mg} (=Mg/(Mg+Fe)), pyrope, grossular, spessartine, almandine, Y, Ti, and P along the line shown in (a). Note that Y, Ti, and P are in app. ppm. (h-j) Core-to-rim laser ICP-MS zoning profiles for Sc, V, Co, Zr, Sm, Gd and Yb. The letter A represents a compositional break defined by a peak in the Y profile.

creases continuously from 629 app. ppm in the core to 320 app. ppm in the rim (Fig. 2f). P decreases slightly from 128 app. ppm in the core to 118 app. ppm in the rim (Fig. 2g). Scandium decreases from 215 ppm in the core to 72 ppm in the rim with an inflection that is correlated with the break in Ca and a slight increase in Zr (Figs. 2h, i). Cobalt increases gradually from core to rim (Fig. 2i) and V concentrations do not change significantly from core to rim (Figs. 2h).

Apatite, which appears red in the P map (Fig. 2d), occurs as a matrix mineral, as inclusions in the garnet, and as a cluster of tiny grains along the left resorbed margin of the garnet. The Y concentration of apatite inclusions in garnet is higher than that of matrix apatite, consistent with the observed decreasing Y concentration towards the garnet rim. Secondary apatite in the garnet resorption area has a slightly higher Y concentration than other matrix apatite, implying that this apatite incorporated Y released from the garnet.

The initial growth of garnet in 87-86 is attributed to an epidote-absent reaction such as reaction (3) because of the low Ca content of the garnet and the continuously decreasing Y and HREE inward of the point A. A period of epidote growth during which garnet did not grow or was slightly resorbed may have followed reaction (3). Addition of epidote to the assemblage in reaction (3) led to the growth of garnet by reaction (1), consistent with the observed increases in Ca, Sc and Zr released from epidote. Major element zoning profiles after the Ca break are compatible with the predicted change of garnet and plagioclase compositions along the compression-heating P - T path; X_{Grs} and X_{An} (~ 0.21) are constant (Fig. 2b). The absence of chlorite in the matrix and the evidence that Ca concentration remained high to the rim suggests that chlorite was consumed during growth of the rim outward of the Ca break and that the garnet continued to grow by reaction (2a) along the compression-heating P - T path. Resorption of garnet is restricted to grains adjacent to mica-rich layers, indicating consumption by the reverse of reaction (3) during retrograde metamorphism.

The occurrence of Y and HREE peaks inside the Ca break suggests that at least the first Y and HREE peaks are not related to the breakdown of epidote, although the minor Y and HREE spikes outside the Ca break may have been produced by breakdown of epidote.

87-279 (Garnet-zone). The peak metamorphic assemblage in this sample was garnet + epidote + biotite + plagioclase + muscovite + quartz, with minor tourmaline, apatite, rutile and ilmenite. The garnet grains contain inclusions of

epidote, apatite, quartz, ilmenite and rutile. X-ray maps and zoning profiles for a representative garnet in sample 87-279 are shown in Fig. 3. BSE images and zoning profiles for the four major elements, plus Y and Ti profiles for sixteen other garnet grains from the same thin-section are included in Appendix 1.

The garnet in Fig. 3 has a spessartine-enriched core ($X_{\text{Sps}} = 0.13$) and displays a moderate decrease in X_{Sps} towards the rim with two distinct annuli (Figs. 3a, e). These annuli generally conform to the euhedral outline of the garnet. However, careful examination of the outer annulus reveals that the inner side is embayed in several places (see red arrows in Fig. 3a), whereas the outer side is straight. The locations of embayments on the inner side of the outer annulus are not related to inclusions. Furthermore, the shapes of Mn zoning profiles across the inner and outer annuli are different; the inner annulus is broad and symmetric, whereas the outer annulus is narrower and asymmetric with a steeper slope on the inner side (see Fig. 3e and Appendix). The increase in spessartine content is correlated with an antithetic change in X_{Alm} and X_{Grs} in the outer annulus, but not in the inner annulus (Fig. 3e and Appendix). Finally, Y concentration in the outer annulus varies significantly from 400 to 1100 app. ppm (Figs. i and k in Appendix). All the above features indicate that the inner Mn annulus is a growth feature, whereas the outer Mn annulus was produced by garnet resorption.

Ilmenite is common in the garnet porphyroblasts and in the matrix (Fig. 3a). Analyses of ilmenite inclusions in garnet show that the Mn content of ilmenite varies sympathetically with that of garnet, implying equilibrium between ilmenite and garnet and that ilmenite was not the source of Mn in the annuli. However, ilmenite crystals in the matrix are significantly enriched in MnO (3.0 wt%), even higher than those in the garnet rim (2.32 wt%). Matrix ilmenite is not zoned in Mn. We speculate that manganese in matrix ilmenite may have been enriched by garnet-consuming reactions associated with formation of sulphide minerals. Sulphide minerals locally replace the rim of the garnet (Fig. 3b), but do not occur as inclusions within garnet, implying they were probably formed during retrograde metamorphism. As in garnet 87-86, X_{Grs} of this garnet is slightly lower in the core (0.204) than the rim (0.238), and is correlated with an increase in Sc (Figs. 3e, h). X_{Grs} remains high throughout the garnet, compatible with the presence of epidote in the matrix. However, X_{Grs} increases slightly from point B outward to the outermost rim.

Yttrium is high (1,009 app. ppm) in the core and plummets to about 450 app. ppm toward the rim with a

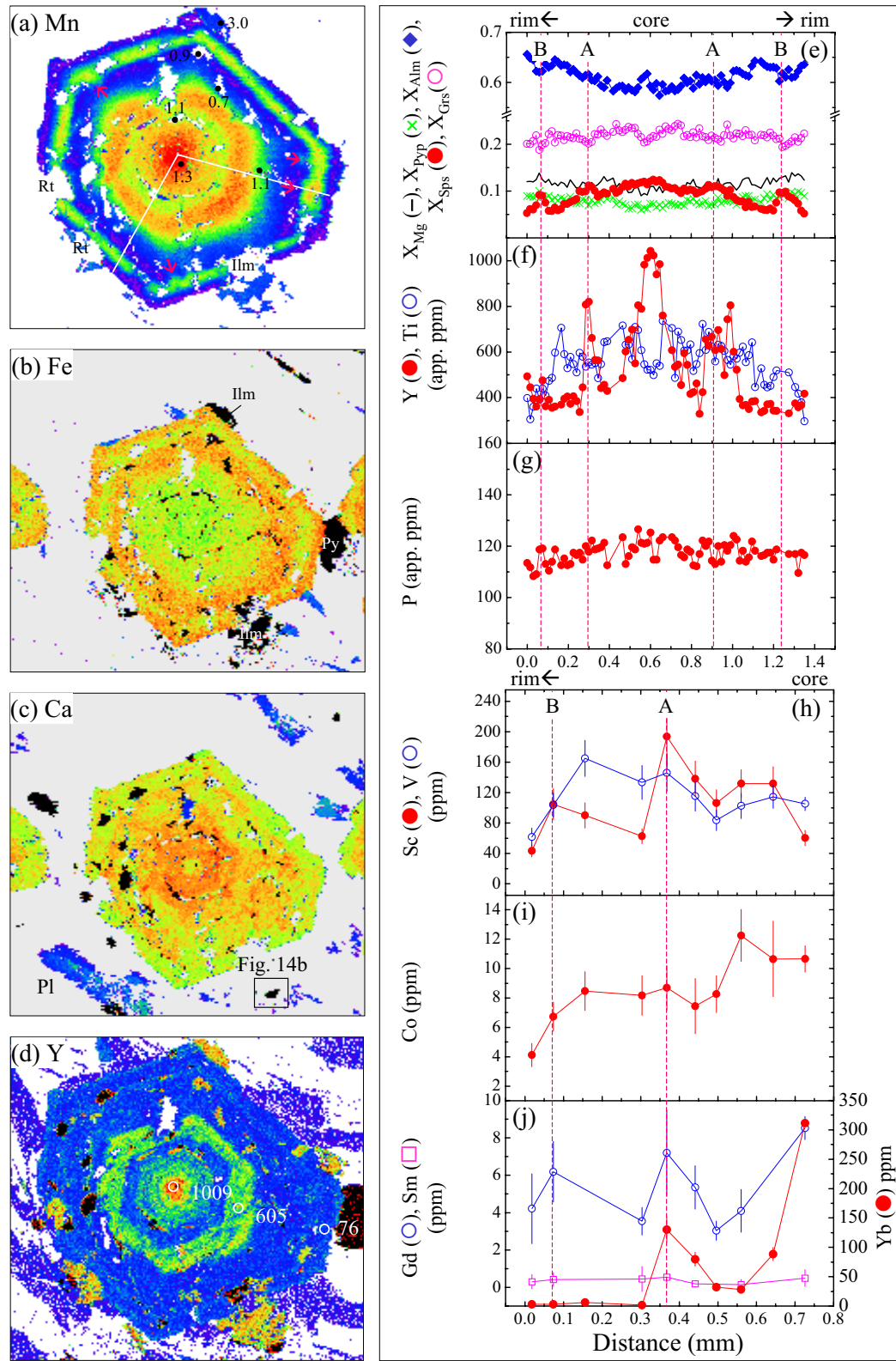


Figure 3. X-ray compositional maps and zoning profiles in garnet from sample 87-279 (garnet zone). (a) Mn map; white lines indicate location of EMP and LAM-ICP-MS profiles. Numbers in Mn map indicate concentrations of MnO (wt. %) in ilmenite. Note that the inner side of the outer Mn annulus is locally embayed as indicated by red arrows. (b) Fe map; note that Fe decreases at the outer Mn annulus, indicating resorption. (c) Ca map; the location of the apatite analyzed in Fig. 14b is indicated by a box. (d) Y map; representative concentrations of Y determined by laser ICP-MS are given in ppm. In the X-ray maps, warm colors indicate higher concentration of MnO, and white for the lowest concentrations. (e-g) Rim-core-rim compositional profiles of X_{Mg} (=Mg/Mg+Fe), pyrope, grossular, spessartine, almandine, Y, Ti, and P along the line shown in (a). Note that Y, Ti, and P are in app. ppm. (h-j) Core-to-rim laser ICP-MS zoning profiles for Sc, V, Co, Sm, Gd and Yb. The letters A and B represent compositional breaks defined by peaks in the Mn profile.

major Y annulus (Figs. 3d, f). The dramatic decrease in Y in the core is similar to Y zoning in garnet produced by breakdown of xenotime in the Bronson Hill Anticlinorium and Merrimack Synclinorium, west-central New Hampshire (Pyle and Spear, 2000). It is interesting to note that in detail the inner annulus may consist of a single peak, or two or more separated peaks, implying a discontinuous supply of Y during the growth of garnet. Although the position of the inner Y annulus coincides with the inner Mn annulus in the garnet in Fig. 3, Y annuli in other garnets in this sample are not always accompanied by an inner Mn annulus, indicating Y may have different sources from Mn (e.g., Figs. a, d, e, i, m, k in Appendix). On the other hand, the outer Mn annulus is correlated with a small increase in Y in several places, supporting the inference that the outer Mn annulus is of resorption origin.

Tiny inclusions (~10 μm) of compositionally zoned, REE-rich epidote in the garnet grains occur outside the low-Ca core (Fig. 4a). In the BSE images of epidote inclusions, light gray zones (1-2 μm wide) have higher Ce

concentrations than the darker areas of the grains, and the zoning pattern appears to reflect a multi-stage growth history prior to partial epidote consumption. Y concentrations also vary greatly across the epidote inclusions, with higher Y contents in the light gray zones, and epidote is not resorbed concentrically, implying that there would have been a discontinuous and irregular supply of Y to the matrix during epidote breakdown. This may explain the observed multiple peaks on the major Y annulus. Growth zoning in other samples can be further complicated by the breakdown of epidote-group minerals such as piemontite, clinozoisite, and allanite which were enclosed in epidote (Figs. 4b, c, d).

Ytterbium and Gd in the garnet in 87-279 exhibit similar behaviour to Y, but Sm shows no significant zoning (Fig. 3j). Ti and P decrease continuously toward the rim in the garnet (Figs. 3f, g), although Ti zoning is disrupted by ilmenite and rutile inclusions. Scandium shows an initial increase in the core and another increase at point A then follows Y, implying that it was derived from the

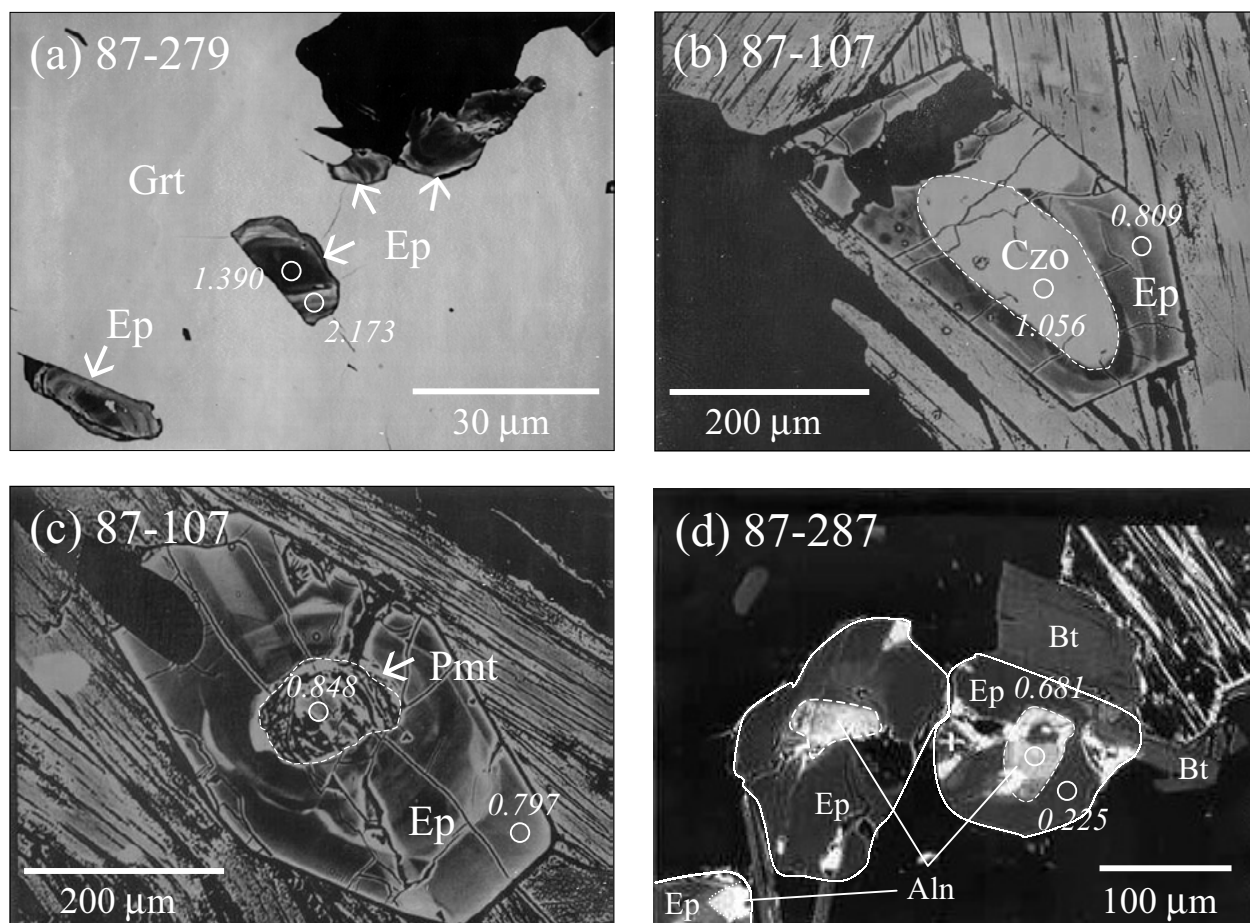


Figure 4. BSE (back-scattered electron) images of epidote-group minerals in Gagnon terrane. The bright areas correspond to high-REE contents. (a) Epidote inclusions in garnet 87-279. (b) Epidote with piemontite-rich clinozoisite core, and (c) epidote with clinozoisite core in sample 87-107 from chlorite-zone. (d) Epidote with allanite core in sample 87-287 from migmatite zone. Numbers in the BSE images indicate Y concentrations in app. wt%.

breakdown of epidote (Fig. 3h). Vanadium concentration increases gradually toward the rim before decreasing at the outermost rim. Unlike garnet 87-86, Co abundance in this garnet decreases toward the rim with no compositional breaks at points A or B.

The core of garnet 87-279 shows the same major and trace element patterns as garnet 87-86; low Ca and Sc and declines in the abundances of garnet-compatible elements such as Y and HREE, suggesting that initial growth of the garnet was by reaction (3). The garnet subsequently grew by reaction (1) as indicated by increases in Ca and Sc derived from breakdown of epidote. At the point B, chlorite was removed from the rock and the garnet was resorbed by reaction (2b), indicating a change of *P-T* path from compression-heating to isobaric heating or decompression. The identity of the reaction that caused renewed growth of garnet outboard of the outer Mn annulus is problematic because both reactions (2b) and (4) consume garnet along the isobaric heating or decompression paths. Renewed growth in the absence of chlorite (reaction 2a) requires an additional period of increasing pressure. This resorption-regrowth of garnet produced the asymmetric Mn and Y zoning profiles with a steeper slope on inner side, which is different from back-diffusion profiles.

87-271 (Staurolite-zone). Sample 87-271 is a staurolite-zone calc-pelite collected from the lowest part of the staurolite-zone (Fig. 1). The matrix assemblage is garnet + biotite + plagioclase + quartz, with no muscovite and staurolite in the matrix. The absence of staurolite in this rock is probably because of either low bulk Al and Fe contents or poor definition of the staurolite isograd in the area. The core, represented by high-Mn ($X_{\text{SpS}} = 0.05$) in the garnet, is not situated in the geometrical center of the grain, implying either asymmetrical growth or that a significant amount of resorption has taken place (Fig. 5a). Resorption is compatible with the corroded appearance of the rim and also with the traditional interpretation of the high-Mn rim ($X_{\text{SpS}} = 0.18$). In addition to the high Mn at the outermost rim, this garnet shows partial preservation of a Mn annulus (red arrows at A, Fig. 5a). It is inferred that most of this Mn annulus was removed by later resorption. A Mn-rich epidote inclusion (~3.83 wt% MnO) was found inside the partial Mn annulus but inclusions of this composition were not found outside the Mn annulus or in the matrix. Severe resorption of the garnet is also indicated by non-concentric Ca zoning and by a thin resorption rim with low Ca (red arrows, Fig. 5b). Grossular is low in the core and increases, then decreases toward the rim. Almandine, which behaves roughly antithetically to grossular in this garnet, decreases sharply at the resorbed rim.

Yttrium and Lu in garnet 87-271 are weakly zoned in the core (Figs. 5f, j) and display an inflection at the point

A where Mn exhibits an annulus. Unlike garnets 87-86 and 87-279, the zone of Y enrichment at the rim of garnet 87-271 is very thin, irregular and discontinuous along the crystal outline and coincides with the low Ca rim zone, consistent with a resorption origin. Gadolinium decreases from 10 ppm in the core to 2 ppm at the point A then increases to 7 ppm at the resorbed rim. Samarium is not zoned in the core of the garnet and decreases outboard of point A.

Garnet in sample 87-271 exhibits a continuous decrease in Ti toward the rim with a significant decrease at the resorbed rim. The abundance of P in the garnet is nearly constant (120 app. ppm). Scandium abundance decreases from the core outward, but increases abruptly outboard of point A. Vanadium is flat in the core and decreases slightly at the rim. Cobalt and Zr increase gradually before decreasing abruptly at the rim.

Most apatite in sample 87-271 occurs inside the original outline of the garnet postulated by Yang and Rivers (2001) on the basis of Cr distribution (see Fig. 5d), implying that apatite was consumed during garnet growth. Apatite crystals occurring in the garnet resorption area have higher Y than apatite inclusions in garnet (Fig. 5d), consistent with growth of apatite at the expense of garnet during resorption.

Major and trace element zoning patterns of garnet 87-271 are similar to those of 87-279; i.e., low Ca and decreasing Y and HREE in the core, a Mn annulus and resorption and regrowth at the rim, the latter inferred from significant increases in Mn, Sc, Y and HREE enrichments at the rim. These features suggest that initial growth of the garnet was by reaction (3), followed by reaction (1) with the addition of epidote in the assemblage. The second increase in Ca can be explained by garnet growth by reaction (2a) along a heating-compression path after chlorite was removed from the assemblage (Table 2). When the *P-T* path changed to isobaric heating, the garnet was consumed by reaction (2b) producing the observed Mn, Sc, Y and HREE enrichments at the rim. Small amounts of garnet grew again by reaction (4) during an inferred second period of compression.

87-287 (Migmatite-zone). In this sample, epidote occurs both as a matrix mineral and as inclusions throughout the garnet. Mn zoning in the core of the garnet is essentially flat, but there is a 500 μm wide incomplete annulus of elevated spessartine inboard from the garnet rim, labeled A in the profile (Figs. 6a, e). The presence of inclusions of Mn-epidote (2.83 wt% MnO) within the annulus suggests that this mineral may be the source of the excess Mn and thus that the annulus is a growth feature,

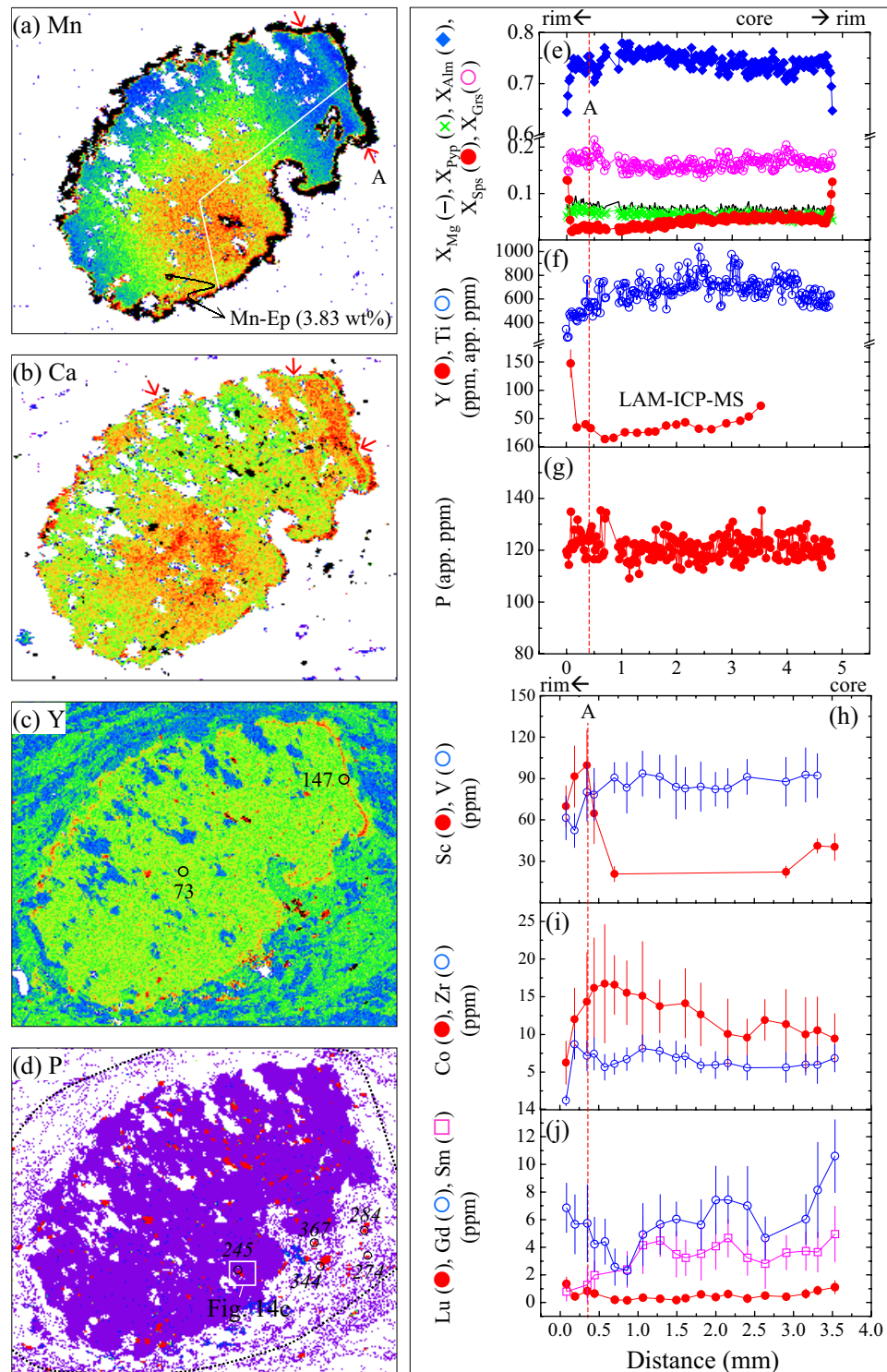


Figure 5. X-ray compositional maps and zoning profiles in garnet from sample 87-271 (stauroilite zone). (a) Mn map; white lines indicate locations of EMP and LAM-ICP-MS profiles. Manganous epidote with 3.83 wt.% MnO occurs in the garnet porphyroblast. The position of a partially preserved Mn annulus is indicated by two red arrows in the upper right corner of the garnet. (b) Ca map; the location of a thin Ca depleted zone is indicated by red arrows. (c) Y map; representative Y concentrations determined by the laser ICP-MS are given in ppm. (d) P map; representative Y analyses of apatite grains are given in app. ppm. Note that the Y concentrations of apatite grains in the garnet resorption area are slightly higher than those of apatite inclusions within the garnet. The location of the apatite shown in Fig. 14c is indicated by a box. Dotted lines represent the postulated former outline of the garnet on the basis of Cr zoning. In the X-ray maps, warm colors indicate higher concentrations with black for the highest and white for the lowest concentrations. (e-g) Rim-core-rim compositional profiles of X_{Mg} (=Mg/Mg+Fe), pyrope, grossular, almandine, Y, Ti, and P along the line shown in (a). Note that Y is in ppm and Ti, and P are in app. ppm. (h-j) Core-to-rim laser ICP-MS zoning profiles for Sc, V, Co, Sm, Gd and Lu. The letter A represents a compositional break defined by the partial Mn annulus

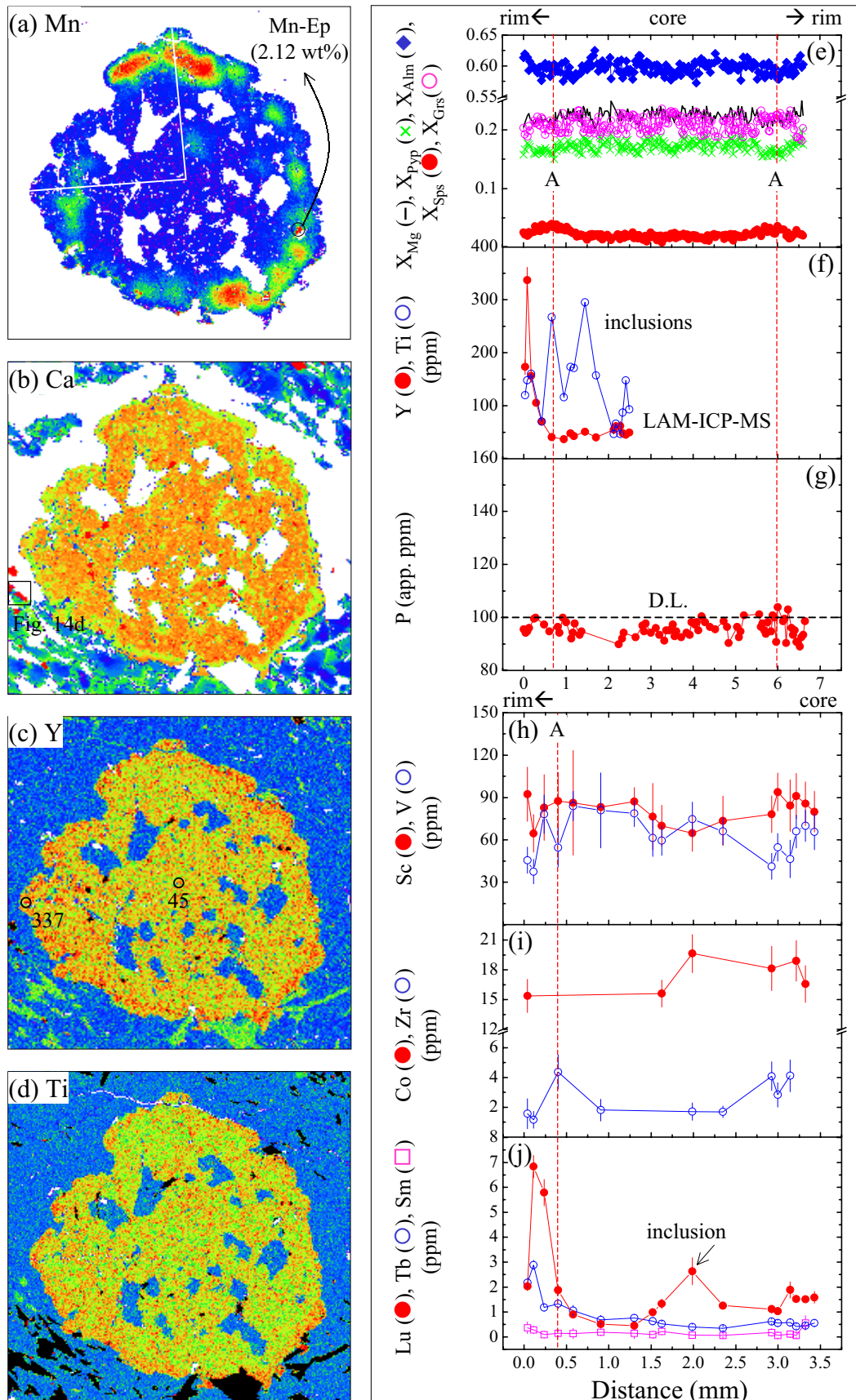


Figure 6. X-ray compositional maps and zoning profiles in garnet from sample 87-287 (migmatitezone). (a) Mn map; white line indicate location of EMP and LAM-ICP-MS profiles. Manganese epidote with 2.12 wt.% MnO occurs within the Mn annulus. (b) Ca map; location of the apatite shown in Figure 14d is indicated by a box. (c) Y map; representative Y concentrations determined by laser ICP-MS are given in ppm. In the X-ray maps, warm colors indicate higher concentrations with black for the highest and white for the lowest concentrations. (e-g) Rim-core-rim compositional profiles of X_{Mg} ($=Mg/(Mg+Fe)$), pyrope, grossular, almandine, Y, Ti, and P along the line shown in (a). Note that Y and Ti are in ppm and P is below the detection limit of electron microprobe analyses. (h-j) Core-to-rim laser ICP-MS zoning profiles for Sc, V, Co, Sm, Tb and Lu. The letter A marks the peak in the Mn profile.

although the Mn annulus is discontinuous. The absence of corresponding Y peaks at the point A support the interpretation that the Mn annulus is not of resorption origin. The absence of Mn and Y enrichment at the outermost rim also suggests that resorption did not occur in this garnet, despite its ragged shape (Fig. 6a), which we therefore infer to be principally a growth feature resulting from pinning of the garnet grain boundary adjacent to quartz and plagioclase, an interpretation compatible with the presence of large quartz inclusions in the centre of the crystal. The grossular component is high (~ 0.20) in the core of the garnet and declines slightly outwards, increasing locally at the rim where garnet is in contact with a plagioclase-rich layer (Figs. 6b, e). The Ca X-ray map shows that X_{An} of plagioclase in the matrix increases from 0.17 in the core to 0.32 in the rim. Neither almandine nor pyrope is significantly zoned.

LAM-ICP-MS analyses of Y and Lu zoning in garnet 87-287 show a slightly enriched core and a sharp increase near the rim to form a narrow annulus with a steeper slope on the outer side, which is a different pattern to that produced by resorption-regrowth (Figs. 6f, j). Terbium displays similar zoning patterns to Y and Lu, except that there is no enrichment in the core (Fig. 6j). Samarium concentration is low in the core (0.1 ppm), but increases by a factor of 4 at the rim (0.4 ppm). Ti zoning roughly parallels that of Y (Figs. 6d, f), and the P content of this garnet is below the detection limit of electron microprobe analysis. Scandium and V in this garnet are essentially unzoned (Fig. 6h), Co decreases toward the rim and Zr shows irregular zoning (Fig. 6i).

There was no change in the mineral assemblage during the garnet growth (Table 1). Numerous inclusions of epidote in the garnet and absence of chlorite in both garnet and matrix indicate that the entire garnet grew by reaction (2a) during a compression-heating P - T path. This interpretation is compatible with the increasing anorthite component in the matrix plagioclase, and the lack of Mn zoning in the core occurs because the isopleths of X_{SpS} are almost parallel to the P - T path for Gagnon terrane (see Fig. 12 of Menard and Spear, 1992).

88-74 (Migmatite-zone). This sample is the only pelitic rock investigated in this study. The garnet in 88-74 displays an oscillatory textural zoning defined by alternating euhedral inclusion-free and inclusion-rich zones (Fig. 7). Parts of this inclusion zonation are truncated at the rim by resorption, especially in the upper right of the garnet. Alternation of inclusion-rich and inclusion-free zones may be explained by a change in the rate of garnet growth (Yang and Rivers, 2001), i.e., garnet growth in the inclusion-rich zones must have been sufficiently rapid

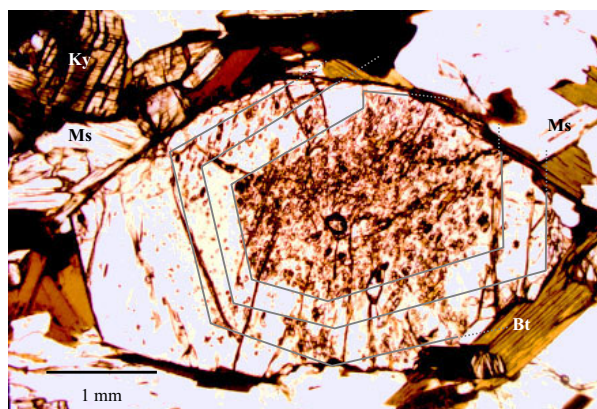


Figure 7. Photomicrograph of sample 88-74 showing the oscillatory textural zoning in garnet defined by alternating inclusion-rich and inclusion-free zones.

to allow entrapment of abundant inclusions. Inclusion phases include quartz, ilmenite, apatite, zircon and rutile (Table 1); xenotime, monazite, and clinozoisite were sought but not found. The matrix surrounding the garnet contains kyanite, biotite, muscovite, quartz, apatite, monazite, zircon, and ilmenite. The spessartine component in this garnet is unzoned in the inclusion-rich core, then decreases monotonically towards the rim before rising at the outermost rim on the left side of the garnet (Figs. 8a, e). Grossular content in the garnet is low (<0.05), compatible with the absence of epidote in this rock, but increases slightly toward the rim before decreasing at the outer rim. Almandine and pyrope are not significantly zoned in the core and their concentrations change antithetically at the rim. A significant amount of resorption is indicated by truncation of high-Ca and -Y bands (Figs. 8b, c).

Yttrium concentration determined by LAM-ICP-MS in the poikiloblastic, inclusion-rich core increases slightly toward the inner inclusion-free zone (Fig. 8f). Yttrium concentration also increases at the beginning of the two inclusion-free zones, and Yb and Gd show similar, but less pronounced variations (Fig. 8j). In contrast to MREE and HREE, Sm and Zr are low (0.34 and 1 ppm, respectively) in the inclusion-rich core and increase in the outer inclusion-rich zone before decreasing again at the outer inclusion-free zone. Titanium zoning is difficult to interpret because many data are contaminated by minute inclusions of Fe-Ti oxides. In this garnet, P increases from 44 app. ppm in the core to 150 app. ppm in the rim, which is almost same as the entire P variation shown by the other six garnets (Fig. 8g). The P increase at the rim is correlated with a decrease in Y, compatible with observations that monazite replaces apatite as the matrix phosphate. Scandium shows a similar zoning pattern to Mn, being high in the core and decreasing toward the rim (Fig. 8h). Vanadium decreases gradually toward the rim, whereas

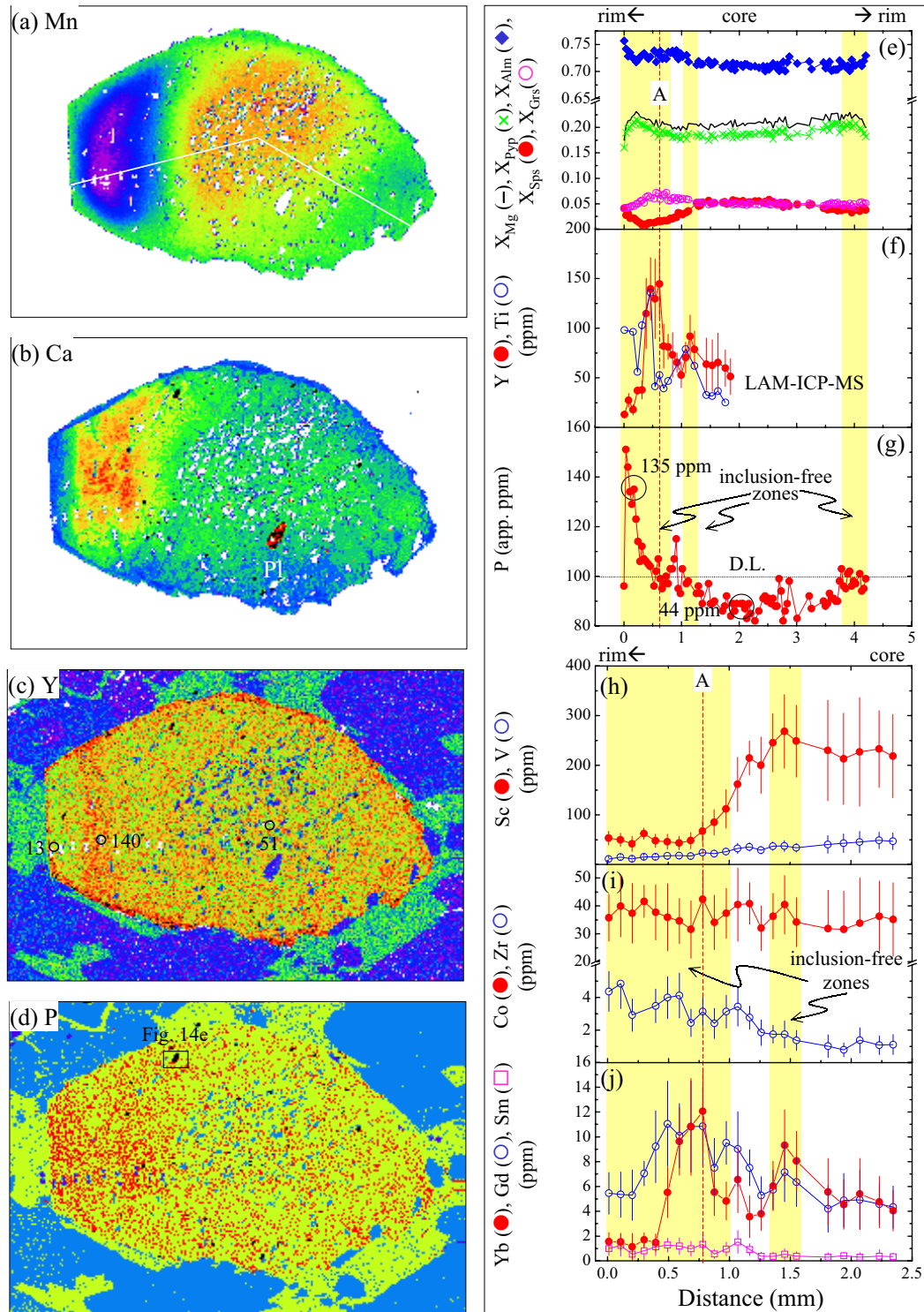


Figure 8. X-ray compositional maps and zoning profiles in garnet from sample 88-74 (migmatite-zone). (a) Mn map; white lines indicate locations of EMP and LAM-ICP-MS zoning profiles. (b) Ca map. (c) Y map: representative concentrations of Y are given in ppm. (d) P map: The location of the apatite in Figure 14e is indicated by a box. In the X-ray maps, warm colors indicate higher concentrations with black for the highest and white for the lowest concentrations. (e-g) Rim-core-rim compositional profiles of X_{Mg} (=Mg/(Mg+Fe)), pyrope, grossular, spessartine, almandine, Y, Ti, and P along the line shown in (a). Note that Y and Ti are in ppm and P is in app. ppm. (h-j) Core-to-rim laser ICP-MS zoning profiles for Sc, V, Co, Zr, Sm, Gd and Yb. The letter A represents a compositional break defined by an abrupt increase in Y. Inclusion-free zones on profiles e-j are shown as vertical yellow bars.

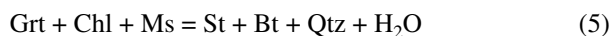
Co and Zr increase continuously toward the rim. In summary, zoning patterns of Zr, Y and REE are correlated with inclusion zoning, and the behaviour of garnet-compatible elements (Y and HREE) is decoupled from garnet-incompatible elements (Sm and Zr) across the oscillatory textural zoning. However, zoning of transition elements (Sc, V, Co) is not correlated with the textural zoning.

88-88 (Migmatite-zone). This garnet also shows an oscillatory textural zoning defined by a euhedral poikiloblastic core, primarily containing inclusions of quartz, apatite, zircon, ilmenite, and rutile, a relatively inclusion-free zone (~300 μm wide), an outer inclusion-rich zone and an inclusion-free rim (Fig. 9). Staurolite, chlorite, epidote, biotite, ilmenite, rutile, apatite and quartz occur as inclusions in this garnet, but epidote inclusions do not occur rimward of the inner inclusion-free zone. Spessartine is high in the core and decreases toward the rim, with a narrow zone of high Mn at the extreme rim (Fig. 10e). However, Mn zoning in the core of the garnet is not concentric (Fig. 10a). This garnet maintains high grossular values (> 0.19) in its core, which fall to below 0.12 at the inner inclusion-free zone, defining the point A in the zoning profiles (Figs. 10b, e). This Ca zoning pattern indicates breakdown of epidote at the point A (see Menard and Spear, 1993). X_{An} is high in the core of pla-



Figure 9. Photomicrograph of sample 88-88 showing the oscillatory textural zoning in garnet defined by alternating inclusion-rich and inclusion-free zones. Bt-biotite, Chl-chlorite, Ky-kyanite, St-staurolite, Tur-tourmaline and Ms-muscovite.

gioclase (0.42) and decreases at the rim (0.37), compatible with the disappearance of epidote at the point A. Almandine and pyrope components show inflections at the inner inclusion-free zone and are decoupled at the outermost rim. X_{Mg} increases sharply at the point A, implying a significant increase in temperature. The presence of staurolite inclusions in garnet suggests that some consumption of garnet must have occurred during staurolite formation by a reaction such as:



Reaction (5) may explain the non-concentric Mn and Ca zoning in the core of the garnet (Figs. 10a, b).

X-ray maps for sample 88-88 display a hexagonal annulus of high-Y that is correlated with the narrow inclusion-free zone and the location of the decline in Ca concentration (Figs. 10c, f). Y concentration increases gradually from the core toward the rim and increases sharply at the point A followed by an immediate decrease. The Y zoning profile shows that the Y concentration along the Y annulus varies from 193 ppm on the left side to 132 ppm on the right side of the profile. Yb and Lu also show peaks coincident with the Y annulus, but unlike Y, REE larger than Tm in ionic radius show initial decreases in their abundance in the core (e.g. Yb in Fig. 10j). Thulium zoning in the core of this garnet is approximately flat (not shown). The shapes of the Y and Yb peaks at the point A are asymmetric, with steeper slopes on their outer sides. Gadolinium also appears to show a similar pattern to Y (Fig. 10j). Samarium is not strongly zoned in the core (0.4 ppm) and increases slightly at the rim (0.8 ppm).

Titanium is high in the core and decreases gradually outward before increasing again at the outer inclusion-rich zone (Fig. 10f). Phosphorus abundance is high in the core (~150 app. ppm) and decreases to ~100 app. ppm at point A, where Ca drops and X_{Mg} increases sharply. Scandium zoning is parallel to that of Ca; i.e., high in the core of the garnet, decreasing abruptly at A (Fig. 10h). Vanadium gradually decreases toward the rim, whereas Co and Zr increase toward the rim with no major breaks in their zoning patterns (Figs. 10h, i). Apatite occurs as inclusions in grains of biotite that replace garnet at the retrograde rim (Fig. 10d). The Y concentrations of some of this apatite are higher than those of apatite elsewhere in the matrix.

88-80 (Migmatite-zone). The analyzed garnet in this sample (8 mm in diameter) is strongly resorbed, as indicated by its ragged appearance (Fig. 11a), and it is mantled by biotite and plagioclase. However, it retains evidence of a large core, defined by enrichment in X_{Sps} and Y with

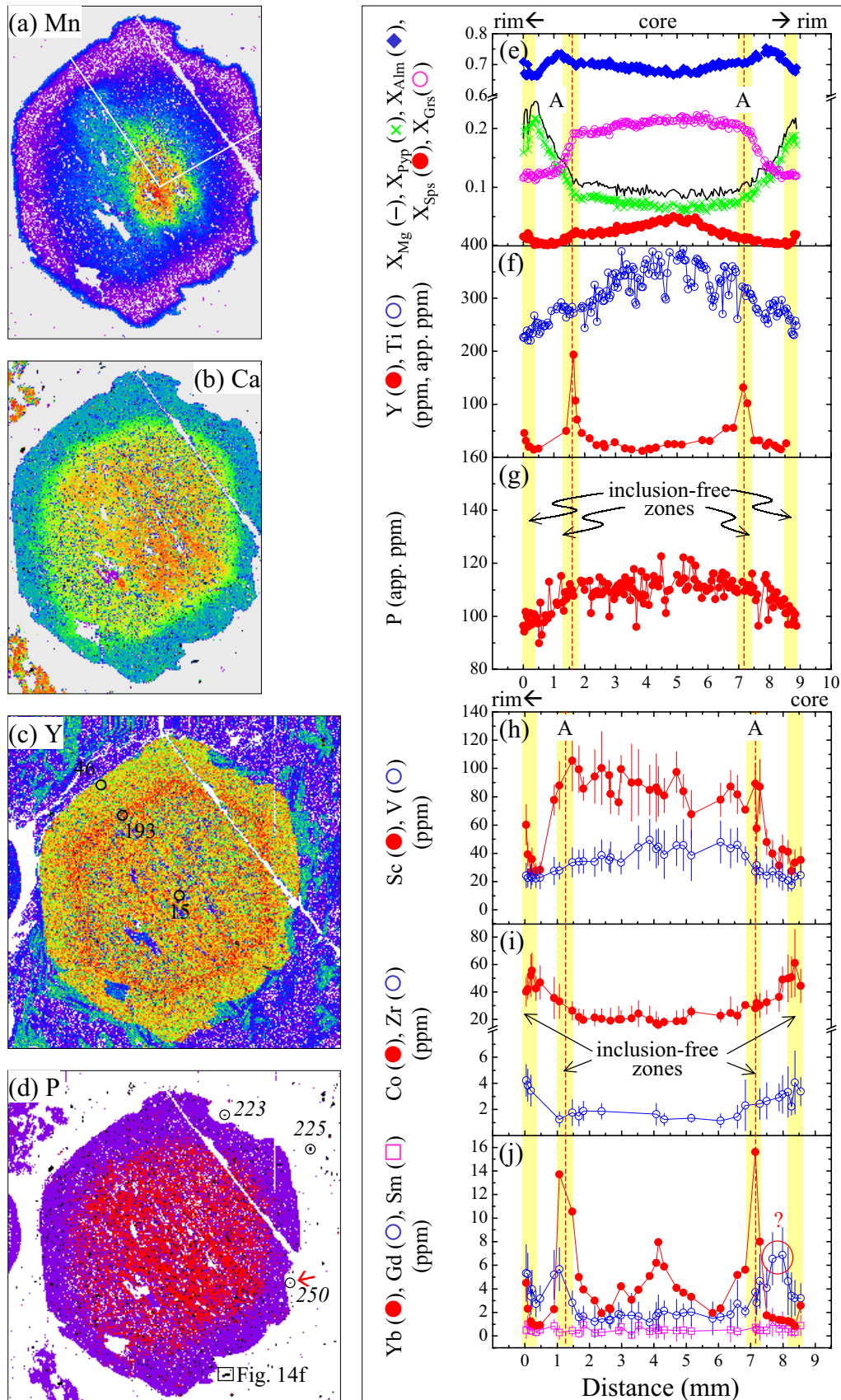


Figure 10. X-ray compositional maps and zoning profiles in garnet from sample 88-88 (migmatite-zone). (a) Mn map; white lines indicate locations of EMP and LAM-ICP-MS profiles. (b) Ca map. (c) Y map: representative Y analyses of apatite grains are given in app. ppm. Note that the Y concentration of apatite in the garnet resorption area (see red arrow) is higher than that of apatite in the matrix. Apatite illustrated in Figure 14f is indicated by box. In the X-ray maps, warm colors indicate higher concentrations with black for the highest and white for the lowest concentrations. (e-g) Rim-core-rim compositional profiles of X_{Mg} (=Mg/(Mg+Fe)), pyrope, grossular, spessartine, almandine, Y, Ti, and P along the line shown in (a). Note that Y is in ppm and Ti and P are in app. ppm. (h-j) Core-to-rim laser ICP-MS zoning profiles for Sc, V, Co, Zr, Sm, Gd and Yb. The letter A represents a compositional break defined by a peak in the Y profile. Inclusion-free zones on profiles e-j are shown as yellow bars.

respect to the rim region (Figs. 11a, c). The Mn growth zoning pattern is truncated by several large quartz grains in and adjacent to the crystal. Yang and Rivers (2001) interpreted these as growth features associated with impingement of matrix quartz on the garnet during growth. The thin elevated Mn rim, which is superimposed on the growth zoning pattern, was caused by minor back diffusion associated with resorption. The Ca map shows an irregular core region with elevated Ca that may also have been affected by the quartz inclusions (Fig. 11b). The grossular component decreases sharply at the rim, and low X_{An} in the core (0.11) of plagioclase is followed by a sharp increase (0.20) at the rim, indicating garnet resorption by reaction (4) during isobaric heating or decompression.

Although this garnet contains epidote inclusions, Y and Lu display typical bell-shaped zoning profiles except adjacent to the large quartz inclusions (Figs. 11f, j). However, slopes of Y and Lu zoning profiles change at the point defined by an inflection in Gd zoning. In contrast, Gd and Sm initially decrease in the core, then increase slightly at point A toward rim (Fig. 11j). The variation of Sm and Gd is also coupled with increases in Sc and Zr, implying breakdown of epidote at point A.

The Ti zoning pattern in garnet 88-80 is difficult to interpret because of numerous minute (< 10 μm in width) rutile and ilmenite inclusions, but it appears to show a gradual increase toward the rim (Fig. 11f). Phosphorus in 88-80 decreases from the core toward point B, then rises steeply towards the rim (Fig. 11g), although no sharp features are preserved in the X-ray map for P (Fig. 11d). This increase in P is correlated with a sharp decrease in Y, as in 88-74, implying a change in the phosphate in equilibrium with garnet from apatite to monazite, compatible with observations. Cobalt in the garnet increases from the core to point B, then decreases at the rim (Fig. 11 i). In contrast, V decreases continuously from 60 ppm at the core to 25 ppm at the rim (Fig. 11h).

Summary of garnet zoning

The patterns of selected major and trace element zoning are schematically depicted in Figure 12 and preliminary interpretations are summarized below. A more complete discussion of the interpretations follows this section.

(a). Typically, Mn is zoned toward lower values outward from garnet cores (samples 87-86, 88-74, 88-88, and 88-80), consistent with depletion of this garnet-compatible element in the matrix during growth of garnet. Samples 87-279, 87-271, and 87-287 are special cases, with several euhedral annuli, a partially preserved Mn annulus near the rim, and a wide Mn-enriched annulus

respectively. The inner Mn annulus in 87-279 does not always correlate with increases in Y and HREE, but Mn annuli in 87-271 and 87-287 are correlated with increases in Y and Zr, respectively. These annuli are interpreted to be growth features because of their euhedral shapes, straight boundaries and the absence of Y annuli produced by resorption and regrowth. The source of the excess Mn is inferred to be Mn-rich epidote (piemontite), probably enclosed in clinozoisite or other matrix minerals.

(b). Garnet porphyroblasts from calc-pelites have high grossular contents, ranging from 0.15 to 0.23 mole fraction, that remained high until epidote breakdown. Constant or slightly decreasing X_{Grs} in most garnets indicates increasing P - T during the growth. Slight increases in Ca in the cores of garnets 87-86, 87-279 and 87-271 mark the breakdown of epidote, an interpretation which is also supported by increases in epidote-compatible elements such as Sc, Y, Zr and REE.

(c). Resorption and regrowth of garnet occurred in samples 87-279 and 87-271 by reaction (2b) along an isobaric heating path, and by reaction (2a) along a compression-heating path. The garnet zoning profiles produced by resorption-regrowth are characterized by asymmetric Mn and Y annuli with steeper slopes and embayed and irregular shapes on their inner sides; those produced during compression-heating are characterized by enrichments in trace elements compatible in epidote (i.e., Y, Sc, HREE).

(d). All the garnets examined, except for sample 88-80, are characterized by Y annuli of variable width (20-300 nm). Sample 88-80 has possibly lost its original Y annulus as a result of subsequent resorption. Although some Y annuli were produced by breakdown of epidote, this interpretation cannot be applied to all analyzed garnets. For example, garnet 87-86 shows Y annuli that formed before the breakdown of epidote, and the breakdown of epidote is not indicated by increases in Y and HREE, but MREE in garnet 88-80. The shapes of Y annuli vary from sharp and euhedral (87-86, 87-279, and 88-88) to anhedral (87-287). The compositional gradient at the Y-peaks may be steeper on the inner side of the peak (outer Y annulus of 87-279, outermost rim of 87-271), or on the outer side of the peak, or be symmetrical (87-86, inner annuli of 87-279, 87-287, 88-74, and 88-88), implying that they have different origins. Most investigated garnets display bell-shaped Y and HREE profiles in their cores (i.e., elements are compatible in garnet), implying initial garnet growth was not associated with epidote breakdown. Variation of Y concentration correlated with textural zoning in samples 88-74 and 88-88 implies control by garnet growth rate.

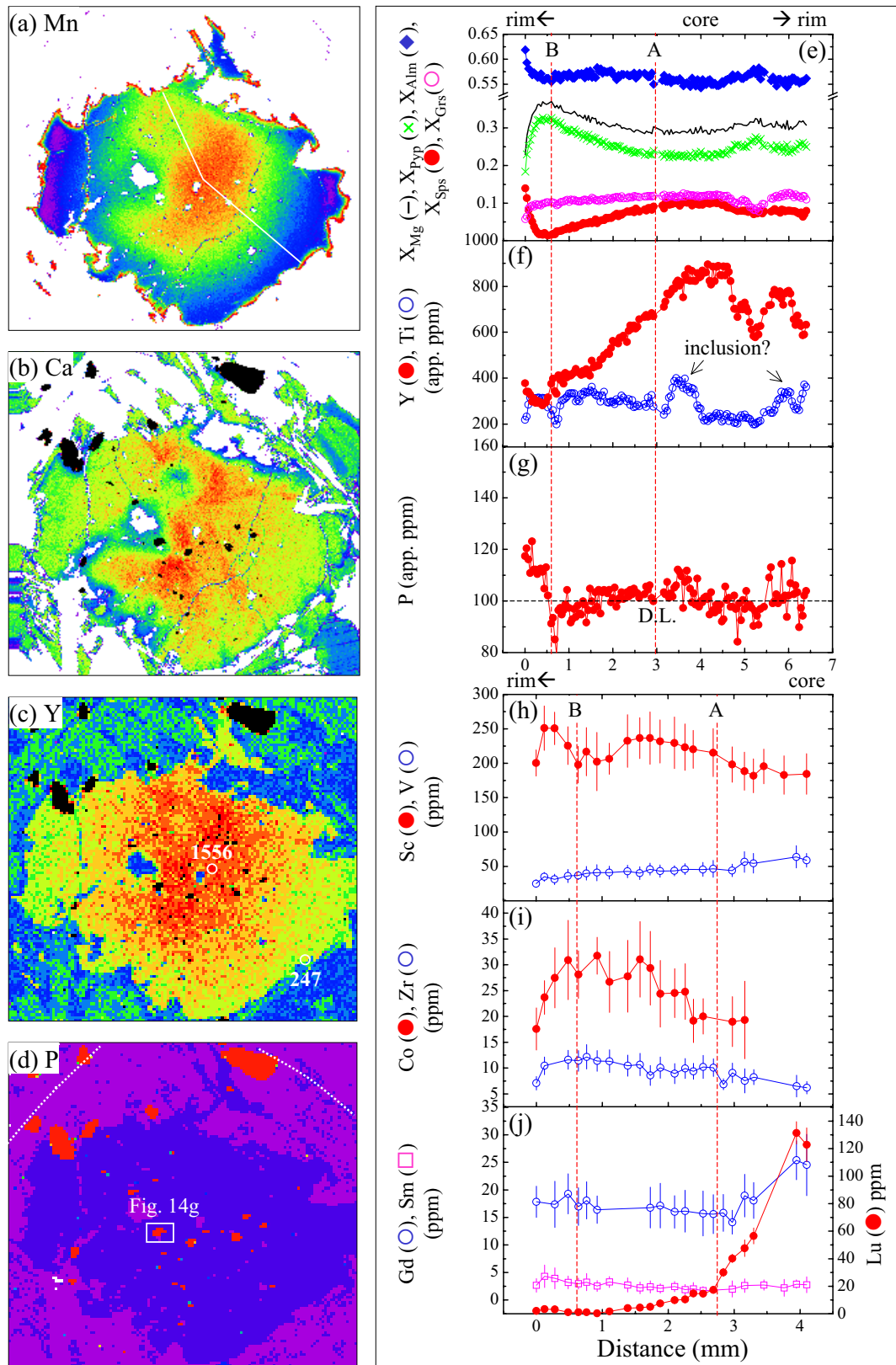


Figure 11. X-ray compositional maps and zoning profiles in garnet from sample 88-80 (migmatite-zone). (a) Mn map; white lines indicate locations of EMP and LAM-ICP-MS profiles. (b) Ca map. (c) Y map; representative concentrations of Y are given in ppm. (d) P map: The location of apatite in Figure 14f is indicated by box. Dotted lines represent the postulated former outline of the garnet on the basis of Cr zoning. In the X-ray maps, warm colors indicate higher concentrations while white for the highest and black for the lowest concentrations. (e-g) Rim-core-rim compositional profiles of X_{Mg} (=Mg/Mg+Fe), pyrope, grossular, almandine, Y, Ti, and P along the line shown in (a). Note that Y, Ti, and P are in app. ppm. (h-j) Core-to-rim laser ICP-MS zoning profiles for Sc, V, Co, Zr, Sm, Gd and Lu. Letters A and B represent compositional breaks defined by inflections in the Gd and P zoning profiles, respectively.

(e). Phosphorus generally shows convex upward profiles, except in samples 88-74 and 88-80, which display sharp increases in P at the rims (Fig. 12). The gradual decrease in P from core to rim in most garnets is correlated with increasing temperature as represented by increases in X_{Mg} toward rims, especially in garnet 88-88. The sharp increases in P at the rims of garnets 88-74 and 88-80 are accompanied by abrupt decreases in Y concentration and appearance of monazite, implying a change in the assemblage which buffers the P-component in garnet.

(f). Scandium profiles from pelitic garnet 88-74 roughly mimic the Mn profiles, implying Sc, like Mn, is compatible in garnet. However, garnet coexisting with epidote shows flat (87-287) or increasing Sc concentration profiles (core of 88-88, 88-80), indicating that Sc is more compatible in epidote than garnet. Scandium peaks coincide with those for Y in epidote-bearing garnets such as 87-86, 87-279, and 87-271, indicating both elements were derived from the breakdown of epidote.

(g). Where analyses are not disrupted by the presence of micro-inclusions, titanium concentration decreases from core to rim in all samples except 88-80. The increasing Ti concentration towards the rim in garnet 88-80 may be a result of changes in the Ti-bearing minor phase assemblage from ilmenite-rutile in the garnet core to rutile in the rim of the garnet, for which there is evidence from the inclusion assemblages (Table 1).

(h). Zirconium increases gradually in abundance from core to rim in garnet in all samples except 87-287, implying that Zr is an incompatible element in garnet. In 87-287, the zoning pattern is less regular and difficult to interpret. Zr is compatible in epidote (Hickmott and Spear, 1992) and Zr profiles show small peaks coincident with Ca or Mn breaks or annuli (e.g., garnet 87-279 and 87-287), implying Zr is an indicator element for reactions involving epidote.

Distribution of REE in epidote and apatite

It is known that chondrite-normalized REE patterns in epidote-group minerals commonly show a marked enrichment of LREE over HREE (Grauch, 1989). On the other hand, it has been reported that epidote and clinzoisite grown from HREE-rich hydrothermal veins show marked enrichment of HREE over LREE (Pan and Fleet, 1996), implying that REE contents in epidote-group minerals may vary greatly depending on external factors such as pressure, temperature, the composition of the coexisting fluid, and phase equilibria with other REE-rich minerals. In this study, an epidote inclusion in garnet from sample P-11 described by Yang and Rivers (2001, see Fig. 1 for location), has a chondrite-normalized REE pattern with a maximum at Tb (MREE) and a slight positive Eu anomaly (Fig. 13). Epidote is also commonly moderately enriched in Sc and V, and strongly enriched in Y and Zr relative to coexisting garnet (Hickmott and Spear 1992; this study).

	X_{Sps}	X_{Grs}	Y	Gd	Sm	P	Sc	Ti	V	Co	Zr
87-86		$\frac{0.19}{0.16}$				$\frac{127}{122}$		$\frac{540}{240}$			$\frac{1.62}{1.62}$
87-279		$\frac{0.23}{0.19}$				$\frac{122}{113}$		$\frac{797}{216}$			$\frac{1.36}{1.36}$
87-271		$\frac{0.20}{0.18}$				$\frac{122}{118}$		$\frac{959}{241}$			$\frac{8.68}{5.96}$
87-287		$\frac{0.21}{0.21}$				< 100		$\frac{138}{47}$			$\frac{4.37}{1.57}$
88-74		$\frac{0.05}{0.05}$				$\frac{153}{44}$		$\frac{96}{25}$			$\frac{4.84}{1.11}$
88-88		$\frac{0.22}{0.12}$				$\frac{113}{<100}$		$\frac{348}{84}$			$\frac{4.21}{1.34}$
88-80		$\frac{0.15}{0.15}$				$\frac{122}{105}$		$\frac{372}{228}$			$\frac{11.61}{6.17}$

Figure 12. Summary of zoning relationships of the analyzed garnets. Italicized numbers for P zoning are in app. ppm. Ti and Zr concentrations (upright numbers) for core and rim are given in ppm.

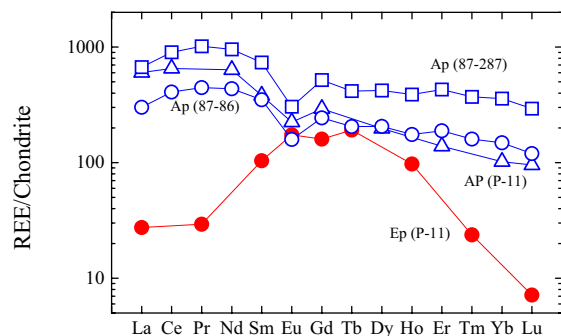


Figure 13. REE patterns of epidote from P-11 (migmatite zone, see Figure 1 and Yang and Rivers, 2001) and apatite from samples 87-86, 87-287, and P-11 normalized to chondrite. Chondrite-normalization factors from Taylor and McLennan (1985).

Representative analyses of apatite crystals performed during the course of this study show LREE-enriched, chondrite-normalized patterns with negative Eu anomalies and variable abundances (Fig. 13).

Distribution of phosphate minerals and Y zoning in apatite

Apatite commonly occurs as subhedral to anhedral grains in our samples, except in sample 88-88 in which it is euhedral to subhedral (Fig. 14). The majority of apatite grains found in the samples are shielded in garnet, especially in migmatite zone samples. These features suggest, together with the presence of measurable P in garnet (40-120 ppm in the analyzed samples) and the convex upward P zoning profiles (Fig. 12), that a significant portion of the apatite was consumed during the growth of the garnet porphyroblasts.

Yttrium zoning in apatite from samples 87-86, 87-287, and 88-88 is flat with similar ranges of Y abundance (~220 app. ppm) in the first two samples and slightly higher (~270 app. ppm) in 88-88 (Figs. 14a, d, f). These Y contents are much lower than in apatite coexisting with xenotime (1,096-1,803 ppm Y) reported from mid-amphibolite-facies metapelite elsewhere (Bea and Montero, 1999). The flat Y zoning and low Y concentrations of apatite from samples 87-86, 87-287, and 88-88, together with the absence of high-Y cores in the coexisting garnets, indicate that xenotime was not present in these rocks and suggest that breakdown of apatite in these samples was not responsible for the observed Y annuli in garnet. In contrast, apatite crystals from samples 87-279, 87-271, and 88-80 are strongly zoned in Y with high Y cores (Figs. 14b, c, g). In addition, LAM-ICP-MS analysis of the core of another apatite in 88-80 indicated a concentration of 997 ppm Y, which is much higher than that shown in Fig. 14g, suggesting that the latter is a non-center cut through the grain. The Y-rich cores of these apatite crystals are

partially exposed to the matrix, indicating that their breakdown could potentially produce Y annuli in growing garnet, depending on the degree of zoning and the modal abundances of apatite and garnet.

The euhedral shape of the high-Y core in apatite from 87-279 (Fig. 14b) indicates that it is a growth feature rather than a detrital core overgrown by a metamorphic apatite. In contrast, the high Y cores in apatite crystals from 87-271 and 88-80 (Figs. 14c, g) are rounded, and it is possible on textural grounds that they are detrital. However, similar ranges of Y concentrations in the cores of all analyzed apatite crystals from the same thin-section, and the absence of a discontinuity in the Y zoning profile of apatite from 88-80 (Fig. 14g), suggest that the high-Y cores in the two apatite crystals are more likely of growth origin. The rounded habit of the apatite cores may have formed by grain boundary migration during metamorphism and deformation. In detail, Y zoning in the cores of apatite crystals from samples 87-279, 87-271, and 88-74 is different from that of sample 88-80; i.e., Y shows a slight increase in the core region in samples 87-279, 88-74, and 87-271, but a continuous decrease in sample 88-80.

The high-Y cores of apatite grains 87-279, 87-271, and 88-74 require breakdown of Y-enriched minerals such as xenotime, monazite, zircon, or garnet during their growth. Among these Y-bearing minerals, xenotime is the only one that can buffer the activity of the Y component in metapelitic apatite (Bea and Montero, 1999; Pyle and Spear, 2000). Xenotime is present in other samples in the area, but not in those examined in this study. Xenotime is consumed in garnet-forming reactions and is an important source of the elevated Y and HREE contents of garnet (Bea and Montero, 1999; Pyle and Spear, 2000). Monazite, another possible source of Y in apatite, does not occur in rocks from the garnet- and staurolite-zones in the study area, which is consistent with observations by Kingsbury et al. (1993), and Rubatto et al. (2001). Monazite and allanite do not coexist in the analyzed samples (Table 1), implying that monazite present as inclusions in metamorphic minerals in the migmatite-zone was produced by the breakdown of allanite and/or apatite (as also documented by others, e.g., Smith and Barreiro, 1990; Ferry, 2000). Monazite can also be produced by reactions involving apatite and LREE-oxides (Akers et al., 1993; Kingsbury et al., 1993; Bingen et al. 1996) or by dissolution-reprecipitation (Rubatto et al., 2001).

Zircon is another possible source of Y in apatite. Zircon occurs in all analyzed samples, and its grain size is approximately constant. Zircons are usually idiomorphic and display oscillatory zoning. Recent age determinations on detrital zircon from metapelite in Gagnon terrane in-

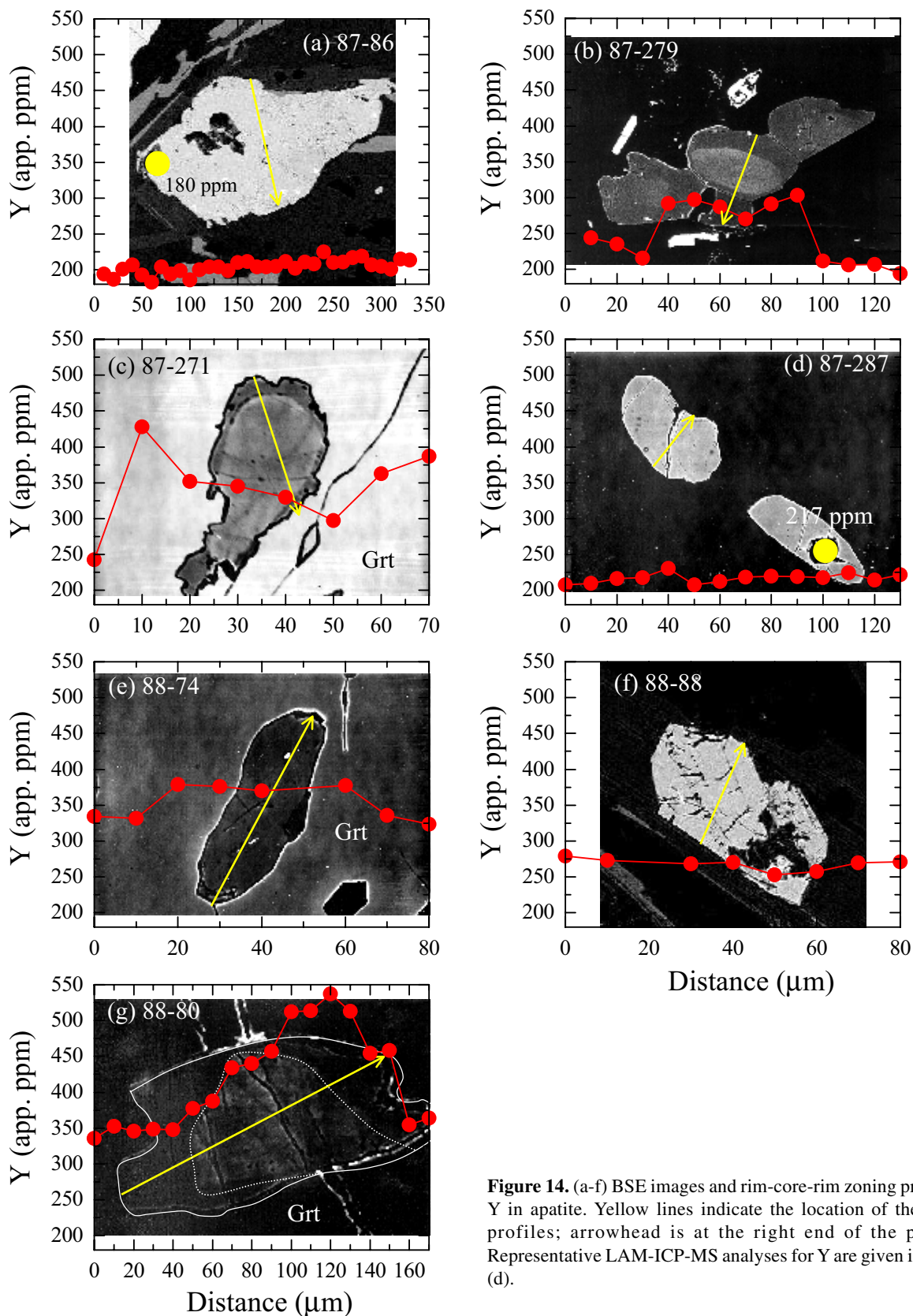


Figure 14. (a-f) BSE images and rim-core-rim zoning profiles of Y in apatite. Yellow lines indicate the location of the zoning profiles; arrowhead is at the right end of the profiles. Representative LAM-ICP-MS analyses for Y are given in (a) and (d).

dicates that most grains retain igneous zoning and yield Archean ages characteristic of their source region (Cox et al. 2001). Only very limited evidence for growth or consumption of zircon during the Grenvillian metamorphism was reported, suggesting that zircon is not likely an important for Y in apatite.

Summarizing the above observations, the high-Y core in apatite in samples 87-279, 87-271, and 88-74 is attributed to crystallization in equilibrium with xenotime, and increasing activity of the Y component in apatite with metamorphic temperature.

The activity of the Y component ($Y_3Al_2Al_3O_{12}$ or YAG) in metapelitic garnet coexisting with xenotime is a function of metamorphic temperature (Pyle and Spear, 2000). This empirical geothermometer can also be used to infer the presence of xenotime in the small Y-rich cores of garnets 87-86 and 87-279. Assuming, *a priori*, the presence of xenotime during the growth of the cores of the two garnets, metamorphic temperatures estimated by the YAG-xenotime thermometer (Pyle and Spear, 2000) for the cores of garnets 87-86 and 87-279 are about 500 and 522°C, respectively. The former temperature is approximately 80°C higher than the estimated garnet core temperature, whereas the latter is in good agreement with the garnet core temperature (both estimates by the garnet-biotite Fe-Mg exchange thermometer). An examination of Y zoning in apatite from these two samples may explain why the result for 87-86 is not in accord with that from Fe-Mg exchange thermometry. Apatite in sample 87-86 has a low Y concentration and flat Y zoning, whereas apatite in 87-279 has a high Y core. This suggests that garnet 87-86 crystallized in a xenotime-absent assemblage, compatible with the spurious temperature estimate with the YAG-xenotime thermometer, whereas xenotime may have been present at the initial stages of garnet growth in sample 87-279. Similarly, the absence of high Y core in garnet 87-271, in which apatite shows the high Y core, may thus indicate that garnet crystallized after the breakdown of xenotime, or that xenotime was armored by other minerals and was not available during the growth of the garnet.

Discussion

Discontinuities in major and trace element zoning in garnet are generally ascribed to some change in the physicochemical environment during garnet growth: e.g., a change in *P-T* conditions, a change in the garnet-forming reaction, a change in the garnet growth rate, a change in garnet major-element composition, or a change in the composition of the coexisting fluid (Hickmott et al., 1987; Hickmott and Shimizu, 1989; Hickmott and Spear, 1992;

Lanzirrotti, 1995; Schwandt et al., 1996; Spear and Kohn, 1996; Bea et al., 1997; Chernoff and Carlson, 1999; Pyle and Spear, 1999). Specific processes that may have influenced the development of P zoning in garnet, Y zoning in apatite and the formation of Mn and Y annuli in the Gagnon garnets are considered below.

Variations of P in garnet and Y in apatite with metamorphic grade

The involvement of apatite in reactions with other phosphates is also indicated. For example, the decrease in modal abundance of apatite with the crystallization of garnet, the presence of trace levels of P in garnet, and the resorbed crystal outlines of apatite crystals, all indicate consumption of apatite during the growth of garnet. On the other hand, small apatite crystals in a garnet resorption area have higher Y concentrations than other matrix apatite, indicating growth of apatite from P, Ca and Y derived from garnet. The involvement of apatite in major mineral reactions is also indicated by Y contents in apatite that were controlled by the breakdown of former xenotime. The appearance and disappearance of trace phases may also reflect changes in metamorphic grade. For example, xenotime starts to break down in the garnet zone (Bea and Montero, 1999; Pyle and Spear, 2000) and allanite-in and monazite-in isograds were recently mapped in a contact aureole (Ferry, 2000).

Although P and Y occur in garnet and apatite at trace levels, P and both P and Y are major structural constituents of apatite and xenotime, respectively. At equilibrium, the chemical potentials of the P-component in garnet and the Y-component in apatite may be buffered by phase relations among phosphates and other silicates, providing the potential to reveal changes in temperature and/or pressure during garnet and apatite growth. However, phase equilibria buffering the activities of the P-component in garnet and the Y-component in apatite are not well known because of poorly understood P and Y substitutions in amphibolite-facies pelitic garnet and apatite.

The substitution of a trivalent species, like Y^{3+} , for Ca^{2+} in the apatite structure must be coupled with another substitution to maintain charge balance. Several such substitutions have been proposed for Y and trivalent REE (Rønso, 1989). These include $Y^{3+} + Si^{4+} = Ca^{2+} + P^{5+}$, $Y^{3+} + Na^+ = 2Ca^{2+}$, $Y^{3+} + O^{2-} = Ca^{2+} + X^-$, and $2Y^{3+} + o = 3Ca^{2+}$ where X is an anion, and o represents a vacancy. Several studies have shown that the first two coupled substitutions dominate in natural apatite (e.g., Rønso, 1989; Fleet and Pan, 1995), and an experimental investigation by Ito (1968) demonstrated the existence of complete solid solution between apatite [$Ca_5(PO_4)_3(F,OH)$] and yttrium-lessingite [$Ca_2Y_3(SiO_4)_3(F,OH)$] under experimental hy-

drothermal conditions (500-700°C, 2 kbar). However, the analytical techniques used in this study are not capable of detecting the dominant substitution.

Although the substitution of Y into the apatite structure and a phase equilibrium accounting for the buffering of the Y-component in apatite are not defined, considerations of the Y zoning pattern of apatite and variation of Y concentration in apatite with metamorphic grade are informative. If the high-Y cores of apatite crystals from samples 87-279, 87-271, and 88-80 were a result of buffering of the Y-component by xenotime, the concentrations of Y in the cores of coexisting apatite could be expected to show temperature dependence in the same way that the Y concentration in monazite or garnet coexisting with xenotime shows a thermal dependence (Pyle and Spear, 2000). Y concentrations in the high-Y cores of apatite vary from ~300 app. ppm in the garnet zone (87-279), through ~440 app. ppm in the staurolite zone (87-271), to 997 ppm in the migmatite zone (88-80). Increasing activity of the Y-component in apatite with metamorphic grade is also consistent with the initial increase in Y concentration in the cores of the apatite in 87-279 and 87-271.

Phosphorus concentration varies smoothly from core to rim in most analyzed garnets. Apparent deviations from this trend are observed in garnets 88-74 and 88-80, where P and Y zoning are decoupled (Fig. 12). In these two samples, monazite was found in the matrix but not in garnet, indicating changes in the coexisting phosphate assemblage from apatite in the garnet cores to apatite + monazite in the garnet rims during garnet growth. Crystallization of monazite at the rims of the two garnets is also compatible with the observed abrupt decreases in Y at the point where P increases. Considering garnet that equilibrated with apatite only, P concentrations at the rims of garnets investigated in this study decrease systematically from a concentration of 122 app. ppm in the garnet zone to about 44 app. ppm in the migmatite zone, except for garnet 87-271, which is significantly resorbed. This systematic variation in P abundance with metamorphic grade and the smooth P zoning with no breaks imply that the activity of the P-component in garnet was buffered by phase equilibria involving apatite and silicates in Gagnon terrane. However, it is difficult to separate the thermal and pressure effects because they vary together in the area, although a significant increase in X_{Mg} in garnet 88-88, accompanied by a sharp decrease in P concentration, indicates that temperature was more likely the dominant factor in controlling P incorporation into garnet.

The substitution mechanism whereby P enters the tetrahedral Z-site in pelitic garnets is not well-known. For pegmatitic garnets, Wise (1994) and Taylor et al. (1997b)

proposed the coupled substitution $2Si^{4+} = P^{5+} + Al^{3+}$ on the basis of strong correlation between tetrahedral silicon deficiency, excess octahedral aluminum, and no appreciable Na in the garnet. For mantle garnet, Sobolev and Lavrent'ev (1971), Thompson (1975), and Bishop et al. (1978) proposed the substitution $Ca^{2+} + Si^{4+} = Na^{+} + P^{5+}$. Since the sum of the atomic radii of Na + P is less than that of Ca + Si, this substitution would cause a shortening of the unit cell edge and a reduction in the unit cell volume, leading Thompson (1975) and Meagher (1982) to propose that it should be sensitive to pressure.

Representative LAM-ICP-MS spot analyses of garnets 87-86 and 88-88 show around 94 and 48 ppm Na, respectively, which are similar to their P abundances, indicating the coupled Na+P substitution is also possible in pelitic garnets. If we consider that the P substitution coupled with Na is preferred by increasing pressure, we would expect to see increasing P concentrations towards the rims of individual garnets, and also higher concentrations of P in the garnets from the highest metamorphic pressure. However, the opposite is observed. P concentrations decrease slightly toward the rims of individual garnets, and there is an overall decrease in P content in garnet with metamorphic grade. We therefore infer that either the temperature effect on P incorporation in garnet was greater than the pressure effect in the analyzed samples, or that the Na + P substitution did not operate in the Gagnon terrane garnets.

Another way of deciphering the relative role of pressure and temperature in P incorporation in garnet is to compare the concentrations of P in garnet that formed under similar temperature, but different pressure conditions. Chernoff and Carlson (1999) reported P zoning in pelitic garnets from the Picuris Range, New Mexico, that equilibrated at about 3.7 kbar and $525 \pm 25^{\circ}C$. We can compare their data with garnet 87-279 (garnet zone), for which estimated conditions of formation are 6 kbar and $550^{\circ}C$. Phosphorus zoning in their garnets is flat in the cores (~100 ppm) then decreases before increasing abruptly to about 200 ppm at a point where Ca shows a spike. Apatite and monazite occur outside the Ca spike but no phosphates were found inside the Ca spike. Assuming that the cores of these garnets grew in equilibrium with former apatite, P concentrations in the garnet cores may be compared to the P concentration in the rim of our garnet 87-279. The similar range of P concentration in garnets from the two areas indicates that temperature may be the factor controlling P incorporation in garnet and that pressure may have a negligible effect.

The apparent P and Y variations in garnet and apatite with pressure and temperature cannot be effectively quantified at this time. However, the decoupling of P and Ca

at the rims of garnets 88-74 and 88-80 suggests that crystal chemistry does not dominate the incorporation of P into garnet. If crystal chemical effects and disequilibrium partitioning can be ruled out, then decreasing P in garnet coexisting with apatite may indicate increasing metamorphic temperature, which is compatible with the observed significant decrease in P concentration with increasing X_{Mg} at the rim of garnet 88-88.

The origin of Mn annuli

We suggested above that breakdown of Mn-rich epidote or allanite was the source of the Mn annuli in garnets 87-271 and 87-287. Enrichment in Mn in the two garnets is correlated with increases in Sc, Zr, Y and M-HREE, which are characteristic signatures of epidote breakdown. Mn from Mn-rich epidote or allanite enclosed in the core of epidote or other matrix minerals was probably released to the matrix at the end of the epidote-breakdown episode (by reactions 1, 2a or 2b), resulting in the formation of Mn annuli near the rims of the two garnets.

The origin of the inner Mn-annulus in sample 87-279, however, is problematic since no Mn-rich mineral was found in this sample. Schumacher et al. (1999) proposed that oscillatory zoning of Mn, decoupled with Fe in their garnet, was due to slight fluctuations in the decompression rate that caused a perturbation of the P - T path and concomitant changes in Fe-Mn exchange be-

tween garnet and ilmenite. Although matrix ilmenite has a high Mn content (~3.0 wt% MnO) in sample 87-279, Mn in ilmenite inclusions in the garnet varies sympathetically with Mn in the host garnet, implying that ilmenite was not the source of the Mn enrichments.

X_{Sps} values at the peaks of the inner annuli in sixteen garnets from sample 87-279 are plotted in Fig. 15. The X_{Sps} is highest in grain e (0.148), with the rest of the garnets analyzed having X_{Sps} between 0.087 and 0.112, with an average of 0.103 ± 0.015 (RSD = 15%). X_{Sps} at the inner annulus also varies within a single garnet grain. For example, garnet grain c shows X_{Sps} values of 0.092 on one side of the annulus and 0.109 on the other side of the same annulus. X_{Sps} values at the inner annulus are low (0.087-0.100) in the upper quartz-rich layer and at the bottom of the thin-section, intermediate (0.100-0.112) in the middle of the garnet-rich area, and very high (0.148) in garnet grain e. This pattern of peak X_{Sps} distribution in the annuli suggests that external infiltration of an Mn-rich fluid or changes in P - T are not likely explanations for the Mn annuli in this sample. Instead, the thin-section scale differences between X_{Sps} values in the annuli suggest that localized breakdown of Mn-rich minerals occurred, either simultaneously or sporadically. Epidote inclusions in garnet 87-279 have very low Mn contents. However, the possibility of Mn-rich epidote in the cores of some of the epidote grains, as in samples 87-271 and

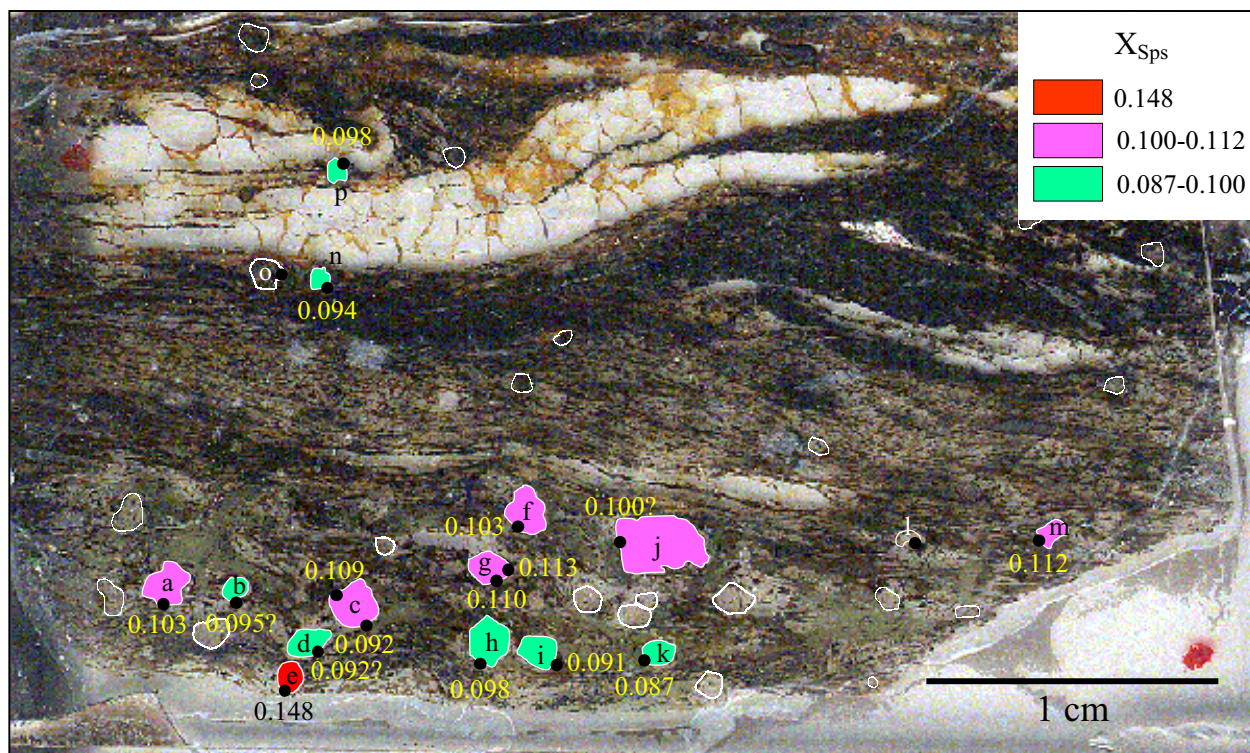


Figure 15. Photomicrograph of sample 87-279 (garnet zone), with 16 garnets colored on the basis of their values of X_{Sps} at the inner annulus.

87-287, or in other minerals, appears likely on the basis of the range of Mn concentrations at the inner Mn-annuli.

The range of X_{Sps} values around an individual annulus also suggests that Mn incorporation into growing garnet rims is controlled by rates of intergranular transport and by local reactions in the immediate vicinity of each garnet porphyroblast. This interpretation is also compatible with the nonsystematic correlation between Mn and Y annuli and with the variable Mn concentrations in the broad annulus in 87-287 (Fig. 6a). Thus, in samples such as this, the use of MnO concentration as an index of the relative time of garnet nucleation (Carlson, 1989; Spear and Daniel, 1998) is questionable, especially where garnet grew at low temperature and in an inhomogeneous matrix with other Mn-rich minerals present.

The origin of Y annuli

High-Y annuli in garnet interiors occur in all the analyzed samples except 88-80, which may have lost its original Y annulus as a result of later resorption. We now consider the origin of this feature, which has the potential to provide important information about the mechanism and history of garnet growth. As noted in the introduction, discontinuous changes in Y and other trace element concentrations in garnet have previously been attributed to: (1) garnet resorption and renewed growth (Pyle and Spear, 1999); (2) disequilibrium partitioning during growth due to kinetic factors such as acceleration of the garnet growth rate (Hickmott and Shimizu, 1990; Lanzirotti, 1995; Chernoff and Carlson, 1999); (3) changes in the garnet-forming reaction due to the breakdown of Y-enriched phases (Hickmott et al., 1987; Hickmott and Spear, 1992; Schwandt et al., 1996; Spear and Kohn, 1996); and (4) infiltration of trace element-enriched fluids during garnet growth (Hickmott et al., 1992; Schwandt et al., 1996; Stowell et al., 1996). Fluid infiltration was suggested by Stowell et al. (1996) to explain oscillatory Y zoning in garnets from contact aureoles surrounding plutons in the Grand Island diorite complex, Alaska. However, it was not considered in this study because indications of an open-system environment as the cause for the Y annuli were not found in the analyzed samples. The single Y annulus observed in most samples is morphologically different from the zoning patterns in garnets that grew in an open-system environment, which tend to show highly variable and irregular patterns of oscillatory zoning, even within a single sample. The three other possible mechanisms are evaluated below.

The shape of Y annuli. As discussed above, the presence of staurolite and epidote in some of these rocks suggests that a significant amount of garnet may have been consumed as a result of reaction (2b) during isobaric heating and reaction (5) along any prograde P - T path. During

garnet resorption, release of garnet-compatible elements such as Mn, Y and HREE would elevate the activity levels of these elements in the matrix and may even stabilize REE-rich minerals such as xenotime (Pyle and Spear, 1999). When garnet begins to grow again, the garnet-compatible elements would again become strongly fractionated into garnet, resulting in an asymmetric annulus with steeper slope on the inner side. On the other hand, garnet-incompatible elements such as Ti, P, V, Co, Zr, and LREE, would enter matrix phases and decline abruptly at the resorbed rim, and then increase gradually during renewed growth. These relationships between garnet-compatible and garnet-incompatible elements are schematically illustrated in Fig. 16. In summary, we predict that resorption and regrowth of garnet would produce a jagged, embayed margin in the garnet with a steeper slope on the inner side of the annulus, as in the garnet rims of samples 87-279 and 87-271 (Figs. 5c, f). However, resorption of garnet may not necessarily produce embayments all around the crystal, as in garnet 87-271 (Fig. 5a), in which they are present on only one side; and in yet other cases, embayments appear to have been localized on crystal defects, e.g., the outer Mn annulus of garnet 87-279 (Fig. 3a).

In contrast, Y annuli produced by growth are characterized by symmetric or asymmetric annuli with a steeper slope on the outer side. If Y zoning is controlled by matrix diffusion, progressive breakdown of an Y-rich trace phase over a temperature or pressure interval will result in an initial gradual increase in Y, as a result of competition for available Y between garnet and the trace phase as the latter breaks down, followed by a sharp decrease in Y after the trace phase is finally consumed (Lanzirotti, 1995). Thus a sudden de-

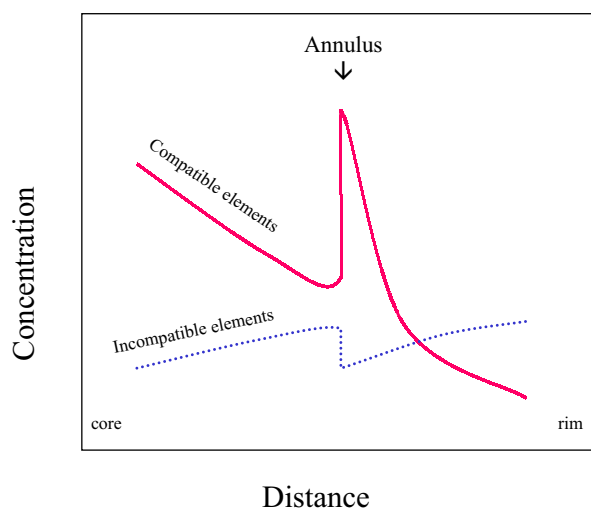


Figure 16. A schematic diagram showing the variation of garnet-compatible and -incompatible elements at an Y annulus formed by garnet resorption and subsequent regrowth.

crease in Y may mark the final breakdown of epidote in sample 87-271.

Another possible mechanism for the gradual increase in Y during breakdown of Y-enriched trace phases is an increase in the effective weight fraction of reactants with increasing metamorphic grade. If the effective weight fraction of matrix minerals increases with temperature due to the logarithmic dependence of diffusion coefficients on temperature, it may produce a gradually increasing concentration of Y toward the rim of garnet even when matrix minerals are not zoned.

Using these criteria, we conclude that the Y annuli in garnets such as 87-86, 87-279 (inner annulus), and 88-88 are not compatible with a resorption model; they display sharp euhedral and straight outlines, the annuli have symmetrical profiles or a steeper slope on the outer side of the peak, and there is non-systematic variation between garnet-compatible and garnet-incompatible elements at the annulus, indicating no garnet resorption or hiatus during the garnet growth. The minerals responsible for the formation of Y annuli in these garnets are discussed below.

Disequilibrium partitioning coupled with change in garnet growth rate. Garnets 88-74 and 88-88 are characterized by oscillatory textural zoning defined by alternating inclusion-rich and inclusion-free zones (Figs. 7, 9). However, breakdown of epidote across the region of oscillatory textural zoning in garnet 88-88 makes the detection of trace element signatures produced by changing garnet growth rates difficult because both processes control Y, Zr and REE zoning. On the other hand, Y and HREE variation in garnet 88-74 can be interpreted largely in terms of changing garnet growth rate because there are no known Y- and HREE-rich minerals in the rock.

For the inclusion-rich zones, it is likely that nucleation of garnet was delayed and significant overstepping of the garnet-forming reactions occurred, resulting in rapid garnet growth with significant trapping of inclusions (Yang and Rivers, 2001). A corollary of the overstepping model is that as the compositions of the reacting minerals approached their equilibrium compositions, the affinity of the reaction would decrease, resulting in slower growth velocity with diminished entrapment of inclusions. However, this would not explain the sharp boundaries between inclusion-rich and inclusion-free zones.

We now consider the effect of rapid growth rate on the incorporation of garnet-compatible elements such as Y and HREE and garnet incompatible elements such as Sm and Zr. Trace element concentrations are known to be enriched in the interfacial regions of polycrystalline ag-

gregates (Kingery, 1984; Watson, 1996). Upon significant increase in growth rate, trace elements bound in the surface layer can be buried and trapped in the newly-formed lattice, resulting in lattice concentrations that deviate substantially from those predicted by equilibrium partitioning between the crystal and its growth medium. The effectiveness of this *disequilibrium growth entrapment process* depends on the interplay between the growth rate of the crystal and the diffusivity in the near-surface region of the crystal. Hickmott and Shimizu (1989) used this argument to explain Ti zoning in garnet from a contact aureole in the Kwoiek area, British Columbia. However, if Y were subjected to such an interface process, its concentration would be expected to decrease, rather than increase at the inclusion-free zones as seen in garnets 88-74 and 88-88.

An alternative mechanism was proposed by Lanzirotti (1995), who suggested that if the supply of elements to the growing garnet interface is diffusion-limited in the matrix, then a decrease in the garnet growth rate will result in an increase in the supply of garnet-compatible elements and a corresponding decrease in garnet-incompatible elements (*diffusion-limited growth*). In garnet 88-74, systematic increases in garnet-compatible elements (Y, HREE, and MREE) at the beginning of each inclusion-free zone and increases in garnet-incompatible elements (Sm and Zr) at the outer inclusion-rich zone provide a robust fingerprint for diffusion-limited incorporation of these elements (Figs. 8f, 10f), indicating that diffusion-controlled growth was predominant over disequilibrium growth entrapment in these samples.

Discontinuous change in the effective bulk composition with respect to Y and REE. Discontinuous breakdown of Y- and REE-enriched refractory trace minerals results in a discontinuous change in the effective bulk composition (EBC) and imparts a characteristic trace element signature on the growing garnet. However, even if breakdown of a trace phase takes place by continuous reactions, for example epidote breakdown by reactions (1) and (2), or the continuous breakdown of apatite indicated by the presence of trace P in the studied garnets implying attainment of equilibrium between garnet and apatite, a similar discontinuous change in the EBC may result. This is because several of the trace minerals are strongly zoned (e.g., epidote), as discussed above, and/or because of inclusions of one phase in another (e.g., inclusions of allanite in epidote).

The signatures resulting from the breakdown of particular trace phases can be predicted from garnet-trace mineral partition data and an understanding of the chemistry of the refractory minerals. Refractory minerals con-

taining significant amounts of Y and REE in the analysed Gagnon calc-pelitic and pelitic rocks include epidote, apatite, monazite, allanite and zircon, with plagioclase as a reservoir for Eu. In this section, we attempt to identify the reactant minerals that produced the Y annuli using REE peaks measured in garnet.

The method of determining REE peaks is shown in Fig. 17a. Essentially, changes in abundances of REE elements are compared at two locations at both the core and annulus (A) regions (referred to as the core and A peaks respectively). The points a and b, and c and d, respectively, are chosen to be as close to each other as analytically possible, thereby fulfilling the conditions of a simple Rayleigh fractionation model and simultaneously minimizing the effect of changes in garnet radius between them. However, when comparing the patterns between the core and annulus regions, it is clear that, for a constant rate of garnet formation, the larger

garnet radius size at the time the annulus formed would result in a greater apparent increase in concentration of the REE elements. Thus, quantitative evaluation of the slopes on the figures between the core and A regions is not directly meaningful, although they have qualitative significance. However, the peaks at particular REEs are independent of the concentrations (and therefore slope), and so provide a qualitative image of the source mineral. Examples of the peaks resulting from the breakdown of monazite, xenotime, epidote and allanite superimposed on a Rayleigh fractionation growth model are shown in Fig. 17b.

Before we apply these principles to our samples, it is also necessary to consider the relative timing of growth of the garnet and the REE- and Y-enriched refractory phase. In general, a refractory REE- and Y-enriched mineral that grew in a closed system *prior* to garnet growth would probably exhibit core to rim depletion in elements highly com-

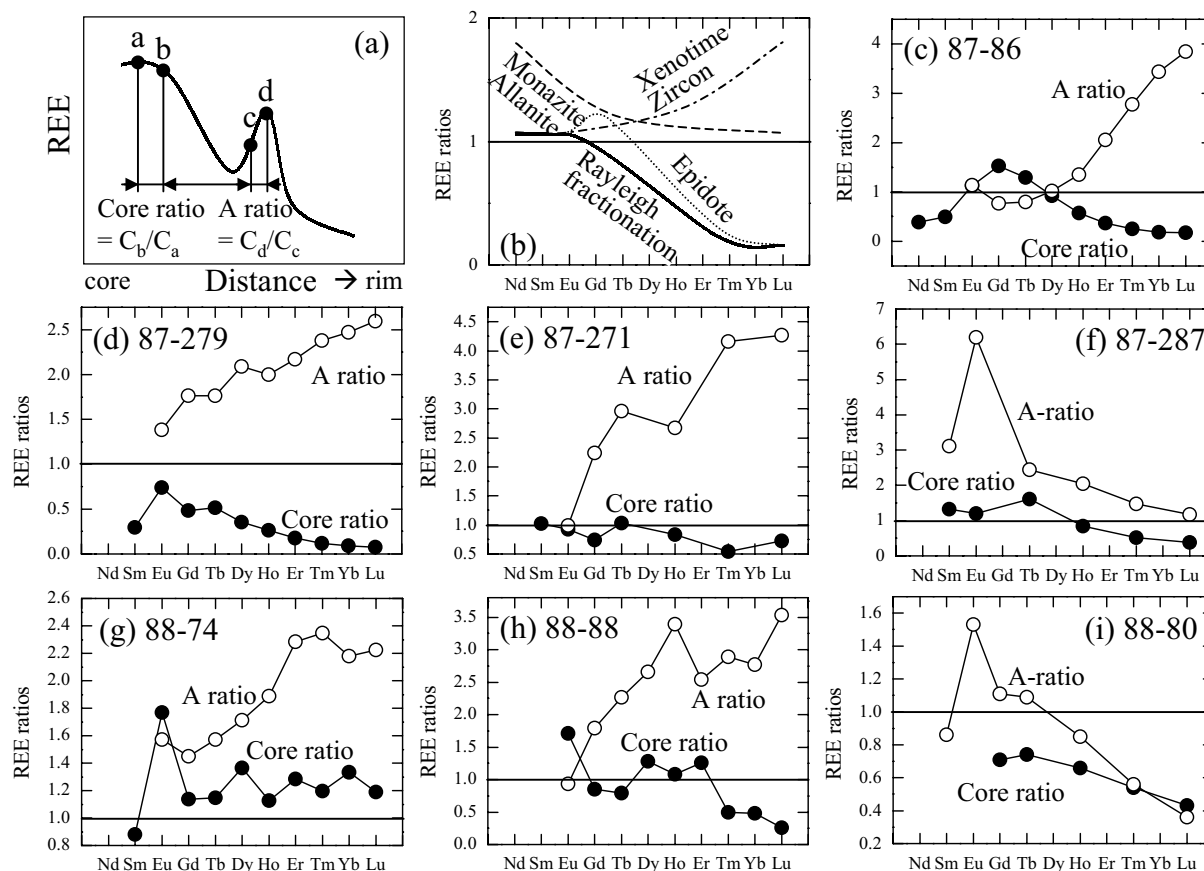


Figure 17. (a) Definition of REE ratios in core and A (annulus) regions of garnet; (b) Hypothetical patterns of REE ratios in garnet: solid line - expected pattern of REE ratios assuming Rayleigh fractionation and a constant EBC; dashed line - pattern of REE ratios where the EBC is modified during garnet growth by the breakdown of a LREE enriched phase (e.g., monazite, allanite); dotted line - pattern of REE ratios where the EBC is modified during garnet growth by the breakdown of a MREE enriched phase (e.g., epidote); dot-dashed line - pattern of REE ratios where the EBC is modified during garnet growth by the breakdown of a HREE enriched phase (e.g., xenotime, zircon). (c-i) Changes in REE ratios in core and A regions in analyzed garnets.

patible in that mineral. On the other hand, any refractory mineral that grew *at the same time as garnet* would exhibit the same core to rim elemental depletions as garnet. Finally, if garnet grew *during the breakdown* of the REE- and Y-rich core of the refractory mineral, then an enrichment of these elements would be observed in the garnet zoning profile. The extent of these effects depends on mass balance constraints and the degree of zoning in the reactant minerals.

Applying these principles to our samples yields the following conclusions. Firstly, with respect to the early stages of garnet growth, core regions of garnets 87-86, 87-287 and 88-88 have peaks in the MREE, Gd, Tb and Dy, respectively, in their core peak plots, compatible with the breakdown of epidote during the initial growth of these garnets (Figs. 17c, f, h). Initial growth of garnets 87-279, 87-271 and 88-80 was not accompanied by epidote breakdown as indicated by all core REE slopes below unity, consistent with the observed initial decrease in Y in the cores of these garnets (Fig. 12 and Figs. 17d, e, i). In garnet 88-74, both MREE and HREE increase slightly during initial garnet growth (Fig. 17g), probably because of reduced garnet growth rate toward the inclusion-free zone. Variation in the Eu slope in the core region is controlled by growth or consumption of plagioclase during the initial growth of the garnets. Positive change of Eu in the core region of garnet 87-279 is compatible with the initial growth of the garnet by reaction (3) in which plagioclase is a reactant, and negative change of Eu in the core region of garnet 87-287 is consistent with growth by reaction (1), in which plagioclase and garnet grow at the expense of epidote.

Having discussed the core peaks, we now turn to the A peaks that are expected to fingerprint the refractory phase that broke down during formation of the Y annuli or inflections in Y concentration in garnet. A-ratio peaks can be classified into four types: (1) peaks at HREE (87-86, 87-279, 88-74), (2) peaks at LREE (87-287), (3) peaks at MREE (88-80) and (4) composite peaks at MREE and HREE (87-271, 88-88). The discontinuous breakdown of xenotime is the most effective method by which the supply of Y and HREE to garnet could have been increased. A-ratio peaks at HREE in garnets such as 87-279, 87-271, 88-88 are compatible with the former presence of xenotime, as also indicated by the high Y cores in coexisting apatite noted above. In addition, the reasonable estimation of temperature using the YAG-xenotime geothermometer (Pyle and Spear, 2000) for the core of garnet 87-279, as discussed above, is also compatible with the former presence of xenotime in this sample. How-

ever, the Y annulus of garnet 87-86 may have been produced by the breakdown of zircon because Y zoning in both garnet and apatite indicate the absence of xenotime in this rock and the Y annulus in garnet before the breakdown of epidote indicates that it was not produced by the breakdown of epidote. A-values for Gd and Tb below unity are also consistent with the REE signature of zircon. HREE-enriched REE peaks of garnet 88-74 imply compatibility differences among REE during a decrease in garnet growth rate.

REE peaks at the Y annulus in garnet 87-287 occur in LREE, indicating breakdown of allanite, apatite or monazite. Apatite in this rock has a low Y concentration (217 ppm) and is not zoned in Y and monazite was not found in this sample. Thus allanite is believed to be the source of LREE enrichment in this case, consistent with remnants of matrix epidote with exposed allanite cores (Fig. 4d). A significant increase in the Eu peak suggests breakdown of plagioclase also occurred during formation of the Y annulus in this garnet.

The location of the A-peak in the LREE to MREE in garnet 88-80 (Fig. 17i) suggests breakdown of epidote at point A, compatible with enrichments in Gd, Sc and Zr. Across the inflection, Y and HREE change slopes in the zoning profiles but the lack of enrichments in these elements suggests that breakdown of epidote does not always increase the level of Y and HREE in the matrix. This may indicate that early epidote, which crystallized before garnet growth, was strongly zoned in Y, and that the Y-poor rims of epidote were involved in garnet formation at point A. Subsequently, with the progress of the epidote-breakdown reaction, the cores of epidote became exposed and released more Y to the EBC.

Two peaks (at MREE and HREE) in garnet 87-271 indicate breakdown of Mn-rich epidote and xenotime at the same time. The presence of xenotime before the crystallization of garnet is indicated by the high-Y core in coexisting apatite, as already noted. The Y annulus in 88-88 is related to the epidote-out reaction, as epidote is restricted to the garnet core inward from the Y annulus. REE variation at the Y-annulus of this sample shows two peaks at MREE and HREE, implying that breakdown of epidote was associated with a breakdown of HREE-enriched mineral such as xenotime and zircon in this sample as well. In summary, the breakdown of Y-enriched cores of epidote, exposure of piemontite or clinozoisite cores in epidote, or the release of epidote group minerals included in other reactant minerals, produced the sharp increases in Y concentration in garnets 87-271, 88-88 and 88-80.

Conclusions

Apatite appears to participate with the major silicate phases in metamorphic reactions in (calc) pelites at all grades. This inference is supported by a decrease in the modal abundance of apatite with garnet growth, the presence of a few hundred ppm P in garnet, convex-upward P zoning in garnet, and the embayed and resorbed outlines of remaining apatite crystals. Garnet coexisting with apatite shows smooth zoning profiles in P and the concentrations of P decrease systematically with metamorphic grade. High Y cores in apatite point to the former existence of xenotime that is inferred to have buffered activity of the Y-component in apatite. In these buffered samples, the Y concentrations in the core increase with metamorphic grade. However, the effects of other phosphates such as monazite and xenotime on P zoning in garnet, P and Y substitutions in garnet and apatite, crystal-chemical effects on Y incorporation in garnet, and the scale of equilibrium all require further evaluation.

Mn annuli are inferred to result from the breakdown of Mn-rich phases such as piemontite (Mn-epidote) during garnet growth. Piemontite-rich inclusions in several of the analyzed garnets support this interpretation. The concentration of Mn in the Mn annuli is shown to vary around individual annuli in a single garnet and by over 15% among garnets in a single thin section, suggesting that the effective Mn concentration varied significantly across the area of a thin section. This result suggests that the uncritical use of Mn concentration as a time marker during garnet growth may be inappropriate.

Yttrium annuli in the analyzed garnet porphyroblasts are shown to result from three processes: garnet resorption and regrowth, disequilibrium partitioning associated with diffusion-limited availability of Y and REE as a result of rapid garnet growth, and breakdown of Y-enriched trace phases during garnet growth. These processes are fingerprinted as follows. (1) Yttrium annuli produced by *garnet resorption and regrowth* are characterized by irregular, locally embayed shapes on the inner side of the annulus, and by systematic variations between garnet-compatible and garnet-incompatible elements at the Y annulus. (2) Where the Y annulus coincides with inclusion-free zones in a garnet poikiloblast, the concentration of Y in garnet is a function of *diffusion-limited growth*, whereby the availability of Y in the matrix is inversely related in some complex manner to the rate of garnet growth. (3) REE peak variations in garnet are shown to be sensitive indicators of the identity of the *trace minerals involved in garnet formation*. For instance, breakdown of epidote during garnet formation results in a peak in MREE, breakdown of allanite results in a peak in

LREE, and breakdown of xenotime and/or zircon result in a peak in the HREE in the associated growing garnet.

Acknowledgments

This study was funded by NSERC grants to T. Rivers. The original manuscript was significantly improved by the criticisms of the journal reviewers F. Spear, J.M. Ferry and J. Pyle. We are grateful to Maggy Piranian and Mike Tubrett for their help with the electron microprobe and LAM-ICP-MS analyses, respectively.

References cited

- Akers, W. T., Grove, M., Harrison, T. M., and Ryerson, F. J. (1993) The instability of rhabdophane and its unimportance in monazite paragenesis. *Chemical Geology*, 110, 169-176.
- Bea, F. and Montero, P. (1999) Behavior of accessory phases and redistribution of Zr, REE, Y, Th, and U during metamorphism and partial melting of metapelites in the lower crust: An example from the Kinzigite Formation of Ivrea-Verbano, NW Italy. *Geochimica et Cosmochimica Acta*, 63, 1133-1153.
- Bea, F., Montero, P., Garut, G. and Zacharini, F. (1997) Pressure-dependence of rare earth element distribution in amphibolite- and granulite-grade garnets. A LA-ICP-MS study. *Geostandards newsletter*, 21, 253-270.
- Bingen, B., Demaiffe, D., and Hertogen, J. (1996) Redistribution of rare earth elements, thorium, and uranium over accessory minerals in the course of amphibolite to granulite facies metamorphism: The role of apatite and monazite in orthogneisses from southwestern Norway. *Geochimica et Cosmochimica Acta*, 60, 1341-1354.
- Bishop, F. C., Smith, J. V, and Dawson, J. B. (1978) Na, K, P and Ti in garnet, pyroxene and olivine from peridotite and eclogite xenoliths from African kimberlites. *Lithos*, 11, 155-173.
- Brown, D., Rivers, T., and Calon, T. (1992) A structural analysis of a metamorphic fold-thrust belt, northeast Gagnon terrane, Grenville Province. *Canadian Journal of Earth Sciences*, 29, 1915-1927.
- Carlson, W. D. (1989) The significance of intergranular diffusion to the mechanisms and kinetics of porphyroblast crystallization. *Contributions to Mineralogy and Petrology*, 103, 1-24.
- Chernoff, C. B. and Carlson, W. D. (1999) Trace element zoning as a record of chemical disequilibrium during garnet growth. *Geology*, 27, 555-558.
- Cox, A., Rivers, T. and Tubrett, M., (2001) Laser-ablation microprobe (U-Pb) zircon ages from reworked

- basement gneiss and supracrustal metasediment, Gagnon terrane, Grenville province. 11th annual V. M. Goldschmidt Conference, 3792.
- Feenstra, A. and Engi, M. (1998) An experimental study of the Fe-Mn exchange between garnet and ilmenite. *Contributions to Mineralogy and Petrology*, 131, 379-392.
- Ferry, J. M. (2000) Patterns of mineral occurrence in metamorphic rocks. *American Mineralogist*, 85, 1573-1588.
- Ferry, J. M. and Spear, F. S. (1978) Experimental calibration of the partitioning of Fe and Mg between biotite and garnet. *Contributions to Mineralogy and Petrology*, 66, 113-117.
- Fleet, M. E. and Pan Y. (1995) Site preference of rare earth elements in fluorapatite. *American Mineralogist*, 80, 329-335.
- Grauch, R. I. (1989) Rare earth elements in metamorphic rocks. In: *Geochemistry and mineralogy of rare earth elements* (Lipin, B. R. and McKay, G. A., eds). *Reviews in Mineralogy*, 21, 147-167, 1989. Mineralogical Society of America, Washington D. C., United States.
- Hickmott, D. D. and Shimizu, N. (1989) Trace element zoning in garnet from the Kwoiek area, British Columbia: disequilibrium partitioning during garnet growth? *Contributions to Mineralogy and Petrology*, 104, 619-630.
- Hickmott, D. D. and Spear, F. S. (1992) Major- and trace-element zoning in garnets from calcareous pelites in the NW Shelburne Falls quadrangle, Massachusetts: Garnet growth histories in retrograded rocks. *Journal of Petrology*, 33, 965-1005.
- Hickmott, D. D., Shimizu, N., Spear, F. S., and Selverstone, J. (1987) Trace-element zoning in a metamorphic garnet. *Geology*, 15, 573-576.
- Hodges, K. V. and Spear, F. S. (1982) Geothermometry, geobarometry and the Al_2SiO_5 triple point at Mt. Moosilauke, New Hampshire. *American Mineralogist*, 67, 1118-1134.
- Indares, A. (1995) Metamorphic interpretation of high-pressure-temperature metapelites with preserved growth zoning in garnet, eastern Grenville Province, Canadian Shield. *Journal of Metamorphic Geology*, 13, 475-486.
- Ito, J. (1968) Silicate apatites and oxyapatites. *American Mineralogist*, 53, 890-907.
- Kingery, W. D. (1984) Segregation phenomena at surfaces and at grain boundaries in oxides and carbides, *Solid State Ionics*, 12, 29-307.
- Kingsbury, J. A., Miller, C. F., Wooden, J. L., and Harrison, T. M. (1993) Monazite paragenesis and U-Pb systematics in rocks of the eastern Mojave desert, California, USA: implications for thermochronometry. *Chemical Geology*, 110, 147-167.
- Lanzirotti, A. (1995) Yttrium zoning in metamorphic garnets. *Geochimica et Cosmochimica Acta*, 59, 4105-4110.
- Meagher, E. P. (1982) Silicate garnets. In: Ribbe P. H. (ed.), *Orthosilicates*, Mineralogical Society of America, Washington, D. C., volume 5, 25-67.
- Menard, T. and Spear, F. S. (1993) Metamorphism of calcic pelitic schists, Strafford Dome, Vermont: Compositional zoning and reaction history. *Journal of Petrology*, 34, 977-1005.
- Newton, R. C. and Haselton, H. T. (1981) Thermodynamics of the garnet-plagioclase- Al_2SiO_5 -quartz geobarometer. In: Newton R. C. (ed.), *Thermodynamics of Minerals and Melts*. Springer Verlag, New York, 131-147.
- Novak, G. A. and Gibbs, G. V. (1971) The crystal chemistry of the silicate garnets. *American Mineralogist*, 56, 791-825.
- Pan, Y. and Fleet, M. E. (1996) Intrinsic and external controls on the incorporation of rare-earth elements in calc-silicate minerals. *Canadian Mineralogist*, 34, 147-159.
- Pyle, J. M. and Spear, F. S. (1999) Yttrium zoning in garnet: Coupling of major and accessory phases during metamorphic reactions. *Geological Materials Research*, 1, 1-49.
- Pyle, J. M. and Spear, F. S. (2000) An empirical garnet (YAG)-xenotime thermometer. *Contributions to Mineralogy and Petrology*, 138, 51-58.
- Rivers, T. (1983a) Progressive metamorphism of pelitic and quartzo-feldspathic rocks in the Grenville Province of western Labrador - tectonic implications of bathozone 6 assemblages. *Canadian Journal of Earth Sciences*, 20, 1791-1804.
- Rivers, T. (1983b) The northern margin of the Grenville Province in western Labrador: anatomy of an ancient orogenic front. *Precambrian Research*, 22, 41-73.
- Rivers, T, van Gool, J. A. M., and Connelly, J. N. (1993) Contrasting tectonic styles in the northern Grenville province: implications for the dynamics of orogenic fronts. *Geology*, 21, 1127-1130.
- Rønso, J. G. (1989) Coupled substitutions involving REEs and Na and Si in apatites in alkaline rocks from the Ilimaussaq intrusion, South Greenland, and the petrological implications. *American Mineralogist*, 74, 896-901.
- Rubatto, D., Williams, I. S., and Buick I. S. (2001) Zircon and monazite response to prograde metamorphism in the Reynolds Range, central Australia. *Contributions to Mineralogy and Petrology*, 140, 458-468.
- Schwandt, C. S., Papike, J., and Shearer, C. K. (1996) Trace element zoning in pelitic garnet of the Black Hills, South Dakota. *American Mineralogist*, 81,

- 1195-1207.
- Schumacher, R., Rötzler, K., and Maresch, W. V. (1999) Subtle oscillatory zoning in garnet from regional metamorphic phyllites and mica schists, western Erzgebirge, Germany. *Canadian Mineralogist*, 37, 381-402.
- Smith, H. A. and Barreiro, B. (1990) Monazite U-Pb dating of staurolite grade metamorphism in pelitic schists. *Contributions to Mineralogy and Petrology*, 105, 602-615.
- Sobolev, N. V. and Lavrent'ev, J. G. (1971) Isomorphous sodium and samarium diffusion in diopside. *Geochimica et Cosmochimica Acta*, 48, 1589-1608.
- Spear, F. S. (1988) Metamorphic fractional crystallization and internal metasomatism by diffusional homogenization of zoned garnets. *Contributions to Mineralogy and Petrology*, 99, 507-517.
- Spear, F. S. and Kohn, M. J. (1996) Trace element zoning in garnet as a monitor of crustal melting. *Geology*, 24, 1099-1102.
- Spear, F. S. and Daniel, C. G. (1998) Three-dimensional imaging of garnet porphyroblast sizes and chemical zoning: Nucleation and growth history in the garnet zone. *Geological Materials Research*, 1, No. 1, 1-44.
- Stowell, H. H., Menard, T., and Ridgway, C. K. (1996) Ca-metasomatism and chemical zonation of garnet in contact-metamorphic aureoles, Juneau gold belt, southeastern Alaska. *Canadian Mineralogist*, 34, 1195-1209.
- Thompson, R. N. (1975) Is upper-mantle phosphorus contained in sodic garnet? *Earth and Planetary Science Letters*, 26, 417-424.
- Taylor, S. R. and McLennan, S. M. (1985) *The continental crust: Its composition and evolution*. Blackwell Scientific, Boston.
- Taylor, R. P., Jackson, S. E., Longerich, H. P., and Webster, J. D. (1997a) In situ trace-element analysis of individual silicate melt inclusions by laser ablation microprobe-inductively coupled plasma-mass spectrometry (LAM-ICP-MS). *Geochimica et Cosmochimica Acta*, 61, 2559-2567.
- Taylor, L., Wise, M. A., Simmons, W. B., and Falster, A. U. (1997b) Occurrence of phosphorus in garnets from gem-bearing pegmatites. *Rocks and Minerals*, 72, 189-190.
- van Gool, J. A. M. (1992) The thermotectonic development of the Grenville Front fold-and-thrust belt in southwestern Labrador. Ph. D. thesis, Memorial University of Newfoundland.
- van Gool, J. A. M. and Cawood, P. A. (1994) Frontal vs. Basal accretion and contrasting particle paths in metamorphic thrust belts. *Geology*, 22, 51-54.
- van Westrenen, W., Blundy, J., and Wood, B. (1999) Crystal-chemical controls on trace element partitioning between garnet and anhydrous silicate melt. *American Mineralogist*, 84, 838-847.
- Watson, E. B. (1996) Surface enrichment and trace-element uptake during crystal growth. *Geochimica et Cosmochimica Acta*, 60, 5013-5020.
- Wise, M. A. (1994) Phosphorus in pegmatitic garnets - examples from Maine. *International Mineralogical Association. General Meeting 16th, Pisa, Italy. Abstracts*, 441.
- Yang, P. and Rivers, T. (2000) Trace element partitioning between coexisting biotite and muscovite from metamorphic rocks, western Labrador: Structural, compositional and thermal controls. *Geochimica et Cosmochimica Acta*, 64, 1451-1472.
- Yang, P. and Rivers, T. (2001) Chromium and manganese zoning in pelitic garnet and kyanite: Spiral, overprint, and oscillatory (?) zoning patterns and the role of growth rate. *Journal of Metamorphic Geology*, in press.
- Yang, P., Rivers, T., and Jackson, S. (1999) Crystal-chemical and thermal controls on trace-element partitioning between coexisting garnet and biotite in metamorphic rocks from western Labrador. *Canadian Mineralogist*, 37, 443-468

Appendix 1. Garnet zoning profiles in sample 87-279

BSE images and core-to-rim quantitative zoning profiles of Fe, Mg, Mn and Ca and qualitative zoning profiles of Y and Ti determined by electron microprobe in sixteen garnets from sample 87-279. Light gray areas in the BSE images are mainly defined by Y zoning. White lines in the BSE images represent the locations of zoning profiles. The contrast of BSE images is enhanced by using a high beam current (100 nA). Solid and dotted red lines in the profiles represent the locations of the inner and outer Mn annuli, respectively. The inner Mn annuli are characterized by broad and symmetrical shapes. In contrast, the outer Mn annuli are characterized by short wavelength, asymmetric profiles with steeper slopes on the inner side. Locations of these garnets and the Mn concentrations at the inner annuli are given in Fig. 15. Note that the Mn concentrations at the inner annuli are not always higher than those of outer annuli (h, i, k) and the inner Mn annuli are not always accompanied by Y annuli (e, i, k). In contrast, outer Mn annuli are correlated with enrichments in Y.

